Theoretical investigation of magnetoelectric behavior in $BiFeO_3$

P. Ravindran,* R. Vidya, A. Kjekshus, and H. Fjellvåg
Department of Chemistry, University of Oslo, Box 1033, Blindern N-0315, Oslo, Norway

O. Eriksson
Department of Physics, Uppsala University, P.O. Box 530, S-751 21 Uppsala, Sweden

(Received 10 May 2006; revised manuscript received 12 October 2006; published 14 December 2006)

The magnetoelectric behavior of $BiFeO_3$ has been explored on the basis of accurate density functional calculations. We are able to predict structural, electronic, magnetic, and ferroelectric properties of $BiFeO_3$ correctly without including any strong correlation effect in the calculation. Unlike earlier calculations, the equilibrium structural parameters are found to be in very good agreement with the experimental findings. In particular, the present calculation correctly reproduced experimentally observed elongation of cubic perovskitelike lattice along the [111] direction. At high pressure we predicted a pressure-induced structural transition from rhombohedral ($R3c$) to an orthorhombic ($Pnma$) structure. The total-energy calculations at expanded lattice show two lower energy ferroelectric phases (with monoclinic Cm and tetragonal $P4mm$ structures), closer in energy to the ground-state phase. Spin-polarized band-structure calculations show that $BiFeO_3$ will be an insulator in A- and G-type antiferromagnetic phases and a metal in C-type antiferromagnetic, ferromagnetic configurations, and in the nonmagnetic state. Chemical bonding in $BiFeO_3$ has been analyzed using partial density of states, charge density, charge transfer, electron localization function, Born-effective-charge tensor, and crystal orbital Hamiltonian population analyses. Our electron localization function analysis shows that stereochemically active lone-pair electrons are present at the Bi sites which are responsible for displacements of the Bi atoms from the centrosymmetric to the noncentrosymmetric structure and hence the ferroelectricity. A large ferroelectric polarization of 88.7 $\mu C/cm^2$ is predicted in accordance with recent experimental findings, but differing by an order of magnitude from earlier experimental values. The strong spontaneous polarization is related to the large values of the Born-effective charges at the Bi sites along with their large displacement along the [111] direction of the cubic perovskite-type reference structure. Our polarization analysis shows that partial contributions to polarization from the Fe and O atoms almost cancel each other and the net polarization present in $BiFeO_3$ mainly (>98%) originates from Bi atoms. We found that the large scatter in experimentally reported polarization values in $BiFeO_3$ is associated with the large anisotropy in the spontaneous polarization.

DOI: 10.1103/PhysRevB.74.224412 PACS number(s): 78.20.Ls, 78.20.Ci, 74.25.Gz

I. INTRODUCTION

Multiferroic materials have coupled electric, magnetic, and/or structural order parameters that result in simultaneous ferromagnetic, ferroelectric, and/or ferroelastic behavior. The magnetoelectric materials have two order parameters, viz. spontaneous polarization for ferroelectric or antiferroelectric cases and spontaneous magnetization for ferromagnetic, ferrimagnetic, or antiferromagnetic cases. Coupling between the spontaneous polarization and spontaneous magnetization leads to magnetoelectric (ME) effects, in which the magnetization can be tuned by an applied electric field and vice versa. There has been considerable recent interest[1–3] in developing multiferroic materials in which interaction between the magnetic and electronic degrees of freedom allows both charge and spin to be manipulated by applied electric or magnetic field.[4,5] These materials have opportunities for potential applications in information storage, the emerging field of spintronics, and sensors. Other potential applications include multiple state memory elements, in which data are stored both in the electric and the magnetic polarizations, or novel memory media which might allow writing of a ferroelectric data bit, and reading of the magnetic field generated by association. Besides the potential applications, the fundamental physics of magnetoelectric materials is rich and fascinating. Hence the theoretical understanding of the intrinsic physical properties of multiferroic oxides is clearly of great importance for both fundamental science and technological applications.

$BiFeO_3$ is ferroelectric with relatively high Curie temperature (T_C; approximately 1100 K) and exhibits antiferromagnetic behavior with high Néel temperature (T_N; approximately 643 K).[6–8] The Fe magnetic moments are coupled ferromagnetically (F) within the pseudocubic (111) planes and antiferromagnetically (AF) between adjacent planes. If the magnetic moments are oriented perpendicular to the [111] direction, the symmetry also permits a canting of the AF sublattices resulting in a macroscopic magnetization; so-called weak ferromagnetism.[9,10] The magnetic structure of $BiFeO_3$ is, in the first approximation, AF with G-type magnetic ordering (G-AF). But the G-AF has been modified by subjecting it to a long-range modulation, manifesting itself in a cycloidal spiral of $\lambda = 620$ Å length with [110] as the spiral propagation direction and spin rotation within (110) which is unusual for perovskites.[11] $BiFeO_3$ shows the linear magnetoelectric effect, with applied magnetic fields inducing weak F and large increase in polarization.[12] The exhibition of weak magnetism at room temperature is due to a residual moment from the canted spin structure.[4] A significant magnetization ($\sim 1 \mu_B$ per unit cell), as well as a strong ME coupling, have been reported recently in high quality thin films.[13] Coexist-

ence of ferroelectricity and ferromagnetism has been observed[14] in bulk $BiFeO_3$-$PrFeO_3$-$PbTiO_3$ solid solutions with compositions $0.2BiFeO_3$-$0.2PrFeO_3$-$0.6PbTiO_3$ and $0.4BiFeO_3$-$0.2PrFeO_3$-$0.6PbTiO_3$. Significant dielectric enhancement in ferromagnetic $0.3BiFeO_3$-$0.7SrBi_2Nb_2O_9$ has been reported,[15] for samples synthesized by sintering mechanically activated oxide mixture. Since epitaxial films of $BiFeO_3$ also show large electric polarization ($\sim 158\ \mu C/cm^2$)[16] they are promising candidate materials for ME-device applications.

An important aspect that emerges upon examination[17] of the properties of single-crystal $BiFeO_3$ is that it has a spontaneous polarization that is significantly smaller than the expected value for a ferroelectric with such a high T_C. It was until recently not clear whether this is a result of intrinsic material properties or of limitations imposed by leakage and imperfect material quality in bulk. Enhancement of spontaneous polarization and related properties have been reported[13,16,18] for heteroepitaxially constrained thin films of $BiFeO_3$ recently and more recent theoretical calculations[19,20] also predicated correctly the presence of large polarization in this material. The sizable polarizations in $BiFeO_3$ are consistent with the observed large atomic distortions,[21,22] but apparently inconsistent with earlier studies of bulk $BiFeO_3$,[17,23,24] the origin of these distinction being currently under debate. This is one of the motivations for the present study.

Recent theoretical report on structural behaviors of $BiFeO_3$ using density functional theory (DFT) calculations show considerable deviation from the experimental findings.[13,19] An ideal cubic perovskite-type structure can alternatively be described in a rhombohedral cell with rhombohedral angle $(\alpha_R)=60°$. The low-temperature neutron measurements[25] show $\alpha_R=59.344°$ and 59.35° from single-crystal x-ray-diffraction measurements.[22] This can be rationalized as an elongation of an ideal cubic perovskite-type structure along the [111] direction. In contrast, the hitherto available theoretical results available[13,19] for $BiFeO_3$ conclude with $\alpha_R=60.36°$ which requires compression along the [111] direction of the cubic perovskitelike lattice, just opposite to the experimental findings. In order to find out whether DFT has failed to reproduce the structural parameters correctly for $BiFeO_3$, accurate calculations are needed. This is another motivation for pursuing this work.

Moreover, observation of enhanced polarization in heteroepitaxially constrained thin films of $BiFeO_3$ and the structural analysis[13] suggest an approximately tetragonal structural arrangement with a superimposed monoclinic distortion of about 0.5°. So, it is indeed interesting to look for possible metastable phases with slightly distorted structural arrangements to identify stable structure of the experimentally obtained heteroepitaxially constrained thin films. Also, structural stability studies on $BiFeO_3$ would be useful to identify the paraelectric phase. Total-energy studies on ferroelectric $BiFeO_3$ in different magnetic configurations would give more insight into its magnetic properties. Hence we have made full structural optimization for $BiFeO_3$ in different atomic arrangements also including different magnetic configurations in the calculations.

The "lone pair" in Bi- or Pb-based oxides is believed to form due to the hybridization of 6*s* and 6*p* atomic orbitals with $6s^2$ electrons filling one of the resulting orbitals in Bi or Pb in their oxides. The lone pair is then considered to be chemically inactive, not taking part in the formation of bonds but sterically active. The hybridization causes the lone pair to lose its spherical symmetry and is projected out on one side of the cation, resulting in an asymmetry of the metal coordination and distorted crystal structures. In the present study we have analyzed the occurrence of lone pair and its role on structural stability with the help of charge density, charge transfer, electron localization function, crystal orbital Hamiltonian population, and partial density of states analyses.

The long-range Coulomb interaction plays a crucial role in ferroelectric materials. It is therefore critical to be able to calculate the spontaneous (i.e., zero field) electric polarization **P** as a function of structural degrees of freedom. It has been shown[26,27] that **P** can directly be calculated as a Berry phase of the Bloch states. As for the dependence of **P** upon the structure, the first-order variation of **P** with atomic displacements is given by the dynamic effective charge Z^*, which can be computed either directly using linear-response methods[28] or numerically by finite differences. For the present study Born effective charges were obtained from finite differences of macroscopic polarization induced by small displacements of the atomic sublattices. Recent theoretical reports[19,29] indicated that it is important to include Coulomb correlation effects via the LDA+U approach into the calculation to describe the electronic structure and ferroelectric behavior of $BiFeO_3$. This motivated us to perform accurate DFT calculation to check the possibility of describing electronic structure, magnetism, and ferroelectric behavior of $BiFeO_3$ within the usual DFT framework.

In this paper we report results of first-principle DFT calculations on structural optimization for $BiFeO_3$ in different atomic arrangements and also with different magnetic configurations. Moreover, we investigate structural phase stability, the electronic structure, chemical bonding, magnetism, and ferroelectric properties of $BiFeO_3$. The remainder of this paper is organized as follows. In Sec. II, we describe the structural aspects and the computations involved in the evaluation of structural phase stability, magnetism, and ferroelectric behaviors. In Sec. III we present our results on structural phase stability, electronic structure, chemical bonding, magnetism, and ferroelectricity, and compare the findings with available experimental and theoretical studies. We summarize and conclude in Sec. IV.

II. COMPUTATIONAL DETAILS

First-principles DFT calculations were performed using the Vienna *ab initio* simulation package (VASP),[30] within the projector augmented wave (PAW) method[31] as implemented by Kresse and Joubert.[32] The Kohn-Sham equations[33] were solved self-consistently using an iterative matrix diagonalization method. This is based on a band-by-band preconditioned conjugate gradient[34] method with an improved Pulay mixing[35] to efficiently obtain the ground-state electronic structure. The forces on the atoms were calculated using the Hellmann-Feynman theorem and they are used to perform a conjugate gradient relaxation. Structural optimizations were

continued until the forces on the atoms had converged to less than 1 meV/Å and the pressure on the cell had minimized within the constraint of constant volume. The calculations were performed within periodic boundary conditions allowing the expansion of the crystal wave functions in terms of a plane-wave basis set.

The generalized gradient approximation (GGA) (Ref. 36) includes the effects of local gradients in the charge density for each point which generally gives better equilibrium structural parameters than the local density approximation (LDA). Ferroelectric properties are extremely sensitive to structural parameters (lattice parameters and atom positions) and hence we have used GGA for all our studies. In the basis we treated explicitly 15 valence electrons for Bi ($5d^{10}6s^26p^3$), 14 for Fe ($3p^63d^64s^2$), and 6 for oxygen ($2s^22p^4$). Brillouin-zone integrations are performed with a Gaussian broadening[37] of 0.1 eV during all structural optimizations. These calculations are performed with a $4\times4\times4$ Monkhorst-Pack **k**-point mesh[38] centered at Γ for the ferroelectric $R3c$ structure and similar **k**-point density has been used for all the other structures considered for the present study. One specific problem of these materials is the presence of "computationally unfriendly" atom configurations such as the first-row element oxygen and the transition-metal iron. Both are kinds of atoms which require extra care: either large basis sets within a pseudopotential scheme, or an all-electron scheme. So we have used very large basis set with 875 eV for the plane-wave cutoff. For the **k**-space integrations in the Berry-phase calculations, a uniform $8\times8\times8$ **k**-point mesh was found to be adequate.

$BiFeO_3$ has a rhombohedrally distorted perovskite-type structure with space group $R3c$.[21,22] For the study of structural phase stability we have considered eight closely related potential structure "types:" $BiFeO_3$ (rhombohedral; $R3c$),[22] $CaTiO_3$ (perovskite prototype; cubic; $Fm\bar{3}m$),[39] $KNbO_3$ (tetragonal; $P4mm$),[40] β-$LaCoO_3$ (rhombohedral; $R\bar{3}c$),[41] α-$LaCoO_3$ (monoclinic; $I2/a$),[42] $PbFe_{0.5}Nb_{0.5}O_3$ (monoclinic; Cm),[43] $GdFeO_3$ (orthorhombic; $Pnma$), and $LaVO_3$ (monoclinic; $P2_1/c$).[44] The reasons for choosing these structure types for our calculations are given below. It is experimentally reported that $BiFeO_3$ stabilizes in the rhombohedral $R3c$ and hence it is natural to include this structure variant. This structure which is also adopted by the paraelectric β-$LaCoO_3$ structure can be derived from the ideal cubic perovskite-type structure by rotation of the octahedra along the cubic [111] axis. Since the experimental studies show enhancement of the polarization in heteroepitaxially constrained thin films of $BiFeO_3$, for which the structural analyses[13] suggest an approximately tetragonal crystal structure with a small monoclinic distortion, we considered structural arrangements within space groups $P4mm$ and Cm. Recent experimental studies show that the β-$LaCoO_3$-type rhombohedral structure undergoes a small monoclinic distortion and stabilizes in an α-LaCoO3 type structure.[42] The orthorhombic $GdFeO_3$-type structure arises from the ideal cubic perovskite by tilting of the FeO_6 octahedra around the cubic [110] axis and with small monoclinic distortion one arrives at the $LaVO_3$-type structure.[44] As experimentally reported crystal structure of thin film has small monoclinic distortion, we have considered the monoclinic $I2/a$, Cm, and $P2_1/c$ structures in our investigations.

The structures were fully relaxed for all volumes considered in the present calculations using force as well as stress minimization. Experimentally established structural data were used as input for the calculations. In order to avoid ambiguities regarding the free-energy results we have always used the same energy cutoff and corresponding **k**-grid densities for convergence in all calculations. A criterion of at least 0.01 meV/atom was placed on the self-consistent convergence of the total energy. Brillouin-zone integration was performed with a Gaussian broadening of 0.1 eV during all relaxations. The present type of theoretical approach has recently been successfully applied[45,46] to reproduce experimentally observed ambient- and high-pressure phases of metal hydrides.

The experimental studies show that the ground state of $BiFeO_3$ is AF with a Néel temperature of 643 K.[17,47] A noticeable magnetization ($\sim1\mu_B$ per cell), as well as a strong magnetoelectric coupling have been reported recently in high-quality epitaxial thin films.[13] The Fe magnetic moments are coupled F within the pseudocubic (111) planes and AF between adjacent planes. It has been reported as a long-wavelength spiral spin structure[11] and possibly a small out-of-plane canting due to weak ferromagnetism.[48] Owing to tilting of FeO_6 octahedra, Fe-O-Fe chains are not subtending to an angle of 180°. As the exchange interaction takes place via these Fe-O-Fe chains, canted spin arrangements arise which further lead to antiferromagnetism with weak ferromagnetism. Since the noncollinearity of the magnetic moments appears to be quite minimal, we made the computational simplification to approximate the magnetic structure to a collinear model.

$BiFeO_3$ has three possible AF arrangements depending on the interplane and intraplane couplings within structure. (i) With interplane AF coupling and intraplane F coupling the A-AF structure arises. (ii) The opposite structure, with the interplane F coupling and intraplane AF coupling is called C-AF arrangement. In the C-AF magnetic structure all magnetic atoms have two F and four AF nearest neighbors (vice versa in the case of A-AF). (iii) If both the inter- and intraplane couplings are AF the G-AF arrangement arises. In a G-AF arrangement for an ideal cubic perovskite-type structure, each magnetic atom is surrounded by six AF neighbors. Because of the rhombohedral distortion we were unable to introduce perfect G-AF ordering (see Fig. 1). However, the adopted G-AF magnetic arrangement has perfect AF ordering according to cubic perovskite-type structure along the ac plane and zigzag chains with AF ordering in the bc plane. For the structural phase stability calculations we assumed AF ordering with **q** vector $(0,0,1/2)$ for all structures except for the cubic variant where we have assumed G-AF ordering and for the $R3c$ variant where we considered nonmagnetic, F, A-AF, C-AF, and G-AF orderings.

In order to understand the role of Bi lone pair on the ferroelectric properties of $BiFeO_3$ we have visualized it with the help of electron localization function (ELF). The ELF provides a measure of the local influence of the Pauli repulsion on the behavior of the electrons and permits mapping in real space of core, bonding, and nonbonding regions in a

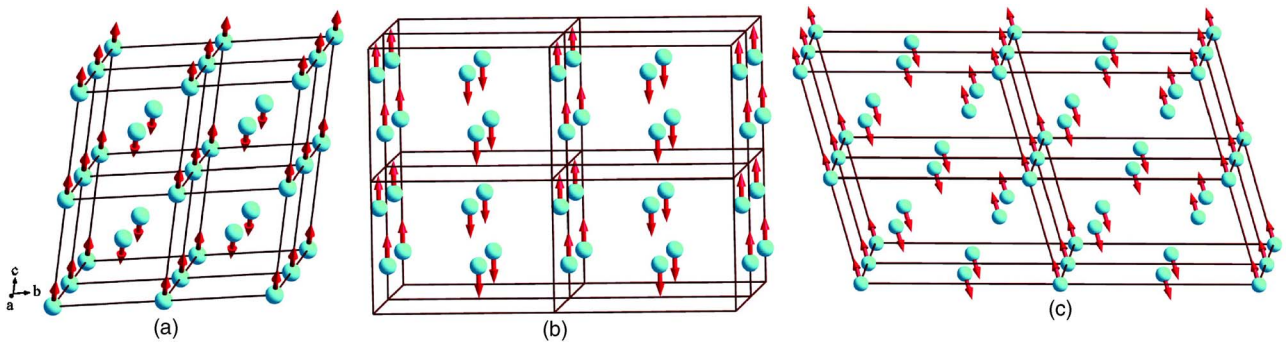

FIG. 1. (Color online) Antiferromagnetic structures considered for ferroelectric $BiFeO_3$ in the (a) *A*-AF-like structure, (b) *C*-AF-like structure, and (c) *G*-AF-like structure. For clarity only the Fe atoms are shown in a $2\times2\times2$ of the primitive cell used in the calculation.

crystal. It can be used to distinguish the nature of different types of bonding in solids.[49] It is defined as

$$ELF = \left[1 + \left(\frac{D}{D_h}\right)^2\right]^{-1}, \quad (1)$$

where

$$D = \frac{1}{2}\sum_i |\nabla\phi_i|^2 - \frac{1}{8}\frac{|\nabla\rho|^2}{\rho}$$

and

$$D_h = \frac{3}{10}(3\pi^2)^{5/3}\rho^{5/3},$$

where ρ is the electron density and ϕ_i are the Kohn-Sham wave functions.

III. RESULTS AND DISCUSSIONS

A. Structural phase stability

$BiFeO_3$ is reported to exhibit about eight structural transitions and a weak F ordering in its ground-state structure.[50,51] The structural instability in perovskitelike oxides is partly related to the lattice mismatch between the cations. Such a mismatch is conveniently quantified in terms of the empirical Goldsmith tolerance factor *t*. It is defined as the ratio between the ideal cubic lattice parameters based on *A*-O vs *B*-O bonding alone, with $t=1$ corresponding to high stability of the cubic perovskite structure. Using the ionic radii given by Shannon and Prewitt,[52] the calculated tolerance factor $[t=(r_{Bi}+r_O)/\sqrt{2}(r_{Fe}+r_O)]$ for $BiFeO_3$ is 0.96. Relatively low value of *t* for $BiFeO_3$ suggests that Bi ion may be unstable in the high-symmetric location possessed by the cubic perovskite-type structure, viz. consistent with the total-energy results discussed below (shown in Fig. 2). In order to minimize the lattice mismatch and gain stability, a lattice distortion arises by the cooperative rotation of FeO_6 octahedra along the [111] direction. In the ideal cubic perovskite structure, the BiO_3 planes are equidistant from the neighboring Fe (111) planes. Due to the rotation of the octahedra, three Bi-O distances are reduced, and three increased, giving rise to an octahedral distortion with rhombohedral symmetry.

The structure of the ferroelectric $BiFeO_3$ phase has been resolved experimentally using x-ray and neutron diffraction,[17,21,22,47,53–55] and found to possess a highly distorted perovskite structure with rhombohedral symmetry and space group $R3c$. The unit cell of $BiFeO_3$ arising from the cubic perovskite structure by two kinds of distortions is shown in Fig. 3. One distortion is the polar displacements of all the anion and cation sublattices relative to each other, which lead to the spontaneous electric polarization, and the other is an antiferrodistortive rotation of the FeO_6 octahedra along the [111] direction with alternating sense of rotation along the [111] axis (owing to the lattice mismatch as mentioned above). In terms of symmetry groups, the polar displacements alone would reduce the symmetry from cubic

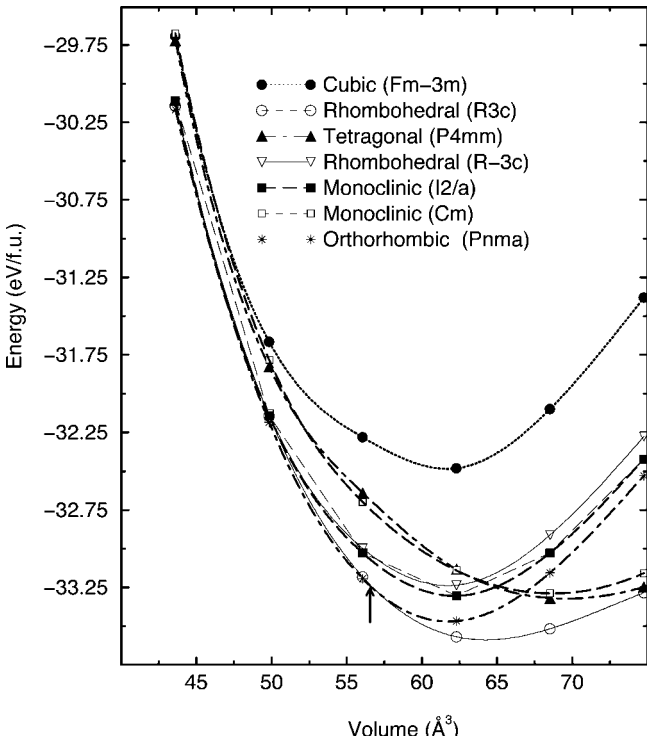

FIG. 2. Calculated cell volume vs total energy for antiferromagnetic $BiFeO_3$ in different possible structural arrangements (structure types being labeled on the illustration). The arrow indicates the pressure-induced structural transition point from the rhombohedral ($R3c$) to the orthorhombic ($Pnma$) structure.

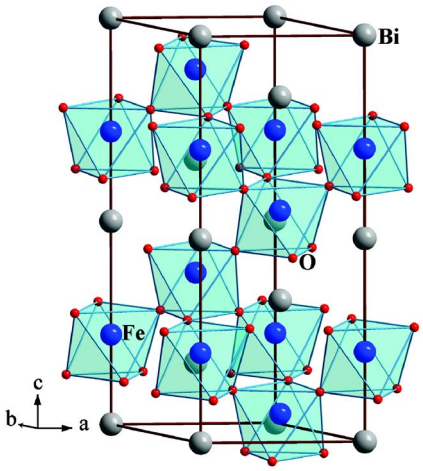

FIG. 3. (Color online) Crystal structure of $BiFeO_3$ in the ferroelectric $R3c$ structures. Highly distorted FeO_6 octahedra are corner shared through oxygen. Also note that Bi atoms are not present exactly in the middle between the FeO_6 octahedra owing to the off-center displacement of Bi due to the presence of 6*s* lone pair electrons.

$Pm\bar{3}m$ to rhombohedral $R3m$, whereas the rotation of the FeO_6 octahedra alone would lead to the paraelectric phase with the space group $R\bar{3}c$. The incorporation of both kinds of distortions gives the actual ferroelectric phase of $BiFeO_3$ with the space group $R3c$.

The calculated total energy vs volume for $BiFeO_3$ in fully relaxed potential structures in the AF states are given in Fig. 2. This figure shows that the experimentally observed ferroelectric $R3c$ phase represents the ground-state structure for $BiFeO_3$. The calculated equilibrium structural parameters for $BiFeO_3$ in the ground state and closely related structures are given in Table I. Our calculated equilibrium structural parameters are also compared with available experimental and theoretical values in this table. The equilibrium volume obtained from the calculation is overestimated compared to the experimental volume by ~3% and the lattice parameters are overestimated by only 1.1%. The overestimation of equilibrium volume by GGA for rhombohedral phase of ferroelectric materials has already been observed for BaTiO3 and PbTiO3,[56] small deviation between experimental and theoretical values indicate the predictive capabilities of the present type of state-of-the-art density functional calculations. It should be noted that the same method with lower energy cutoff and **k**-point densities yielded[19] the equilibrium volume which is much smaller (~6.9%) than the experimental values. An earlier report[13] shows that the ferroelectric properties of $BiFeO_3$ are very sensitive to the small changes in the lattice parameters. So, accurate calculations for the estimation of structural parameters for $BiFeO_3$ are needed in order to predict the ferroelectric properties correctly.

The hypothetical nonferroelectric cubic perovskite-type structure is found to exhibit the highest energy among the various $BiFeO_3$ phases tested in this study. The energy difference between the prototypical cubic structure and the equilibrium ferroelectric $R3c$ structure is around 1.1 eV/f.u. This indicates that the paraelectric phase of $BiFeO_3$ does not take the cubic perovskitelike structure. In fact several low symmetric atomic arrangements based on tetragonal, rhombohedral, and monoclinic structures are found at lower total energy than the cubic perovskite-type structure (see Fig. 2). It is worthy to note that several low symmetry structures are found to be stable at high pressures in the closely related system $PbTiO_3$.[57] The stabilization of low symmetric structures is associated with the presence of lone pair electrons on

TABLE I. Optimized structural parameters (a in Å, α in deg, and equilibrium volume V_0 in $Å^3$) and bulk modulus (B_0 in GPa) for $BiFeO_3$ in different structural arrangements.

Modification (structure type)	Unit cell dimensions	Positional parameters	B_0
$R3c$ (Present, theory)	a=5.697; α=59.235 V_o=128.48	Bi(2*a*): 0, 0, 0; Fe(2*a*): 0.2232, 0.2232, 0.2232 O(6*b*): 0.5342, 0.9357, 0.3865	130.9
$R3c$ (Ref. 19, theory)	a=5.46; α=60.36 V_o=115.98	Bi(2*a*): 0, 0, 0; Fe(2*a*): 0.231, 0.231, 0.231 O(6*b*): 0.542, 0.943, 0.408	
$R3c$ (Ref. 59, theory)	a=5.50; α=59.99 V_o=117.86	Bi(2*a*): 0, 0, 0; Fe(2*a*): 0.228, 0.228, 0.228 O(6*b*): 0.542, 0.942, 0.368	
$R3c$ (Ref. 22, experiment)	a=5.63; α=59.35 V_o=124.60	Bi(2*a*): 0, 0, 0; Fe(2*a*): 0.221, 0.221, 0.221 O(6*b*): 0.538, 0.933, 0.395	
$R\bar{3}c$ (Present, theory)	a=5.513; α=61.432 V_o=122.29	Bi(2*b*): 1/2, 1/2, 1/2; Fe(2*a*): 0, 0, 0 O(6*b*): 0.3358, 0.1641, 1/4	89.8
$R\bar{3}c$ (Ref. 19, theory)	a=5.35; α=61.93 V_o=113.12	Bi(2*b*): 1/2, 1/2, 1/2; Fe(2*a*): 0, 0, 0 O(6*b*): 0.417, 0.083, 1/4	
Pnma (Present, theory)	a=5.5849; b=7.6597; c=5.3497 V_o=113.12	Bi(4*c*): 0.0536, 1/4, 0.98858; Fe(4*b*): 0, 0, 1/2 O(4*c*): 0.9750, 1/4, 0.4060; O(8*d*): 0.2000, 0.9540 0.1945	138.8
*P*4*mm* (Present, theory)	a=3.7859; c=4.8525; V_o=139.10	Bi(1*a*): 0, 0, 0.9491; Fe(1*b*): 1/2, 1/2, 0.51804 O(1*b*): 1/2, 1/2, 0.1428; O(2*c*): 0, 1/2, 0.6735	72.3
Cm (Present, theory)	a=5.7900; b=5.6899; c=4.1739; β=91.99; V_o=137.42	Bi(2*a*): 0.9376, 0, 0.0685; Fe(2*a*): 0.5110, 0, 0.4961 O(2*a*): 0.5626, 0, 0.9489; O(4*b*): 0.7958, 0.7603, 0.4231	79.0

Bi and also the hybridization between Bi and O. At expanded lattice we have identified two ferroelectric structures which are energetically closer to the ground-state structure. One is a tetragonal *P*4*mm* structure and another is a monoclinic *Cm* structure. According to a recent structural refinement by Noheda *et al.*,[58] $PbZr_{0.52}Ti_{0.48}O_3$ (PZT) at 20 K is in the monoclinic *Cm* structure. PZT also stabilizes in the tetragonal *P*4*mm* structure. This material exhibits extremely large electromechanical coupling in both tetragonal and monoclinic phases. It is also interesting to note that enhancement of spontaneous polarization and related properties in heteroepitaxially constrained thin films of $BiFeO_3$ has been recently reported.[13,16,18] In this context observation of metastable *Cm* and *P*4*mm* phases in $BiFeO_3$ is particularly interesting.

The total energy curves in Fig. 2 show that there is a large difference in total energy between considered phases at the expanded lattice. However, at high pressures the energy difference is small which is associated with the weakening of directional bonding at higher pressures. Interestingly we observed a pressure-induced structural transition from the ground state rhombohedral *R*3*c* structure to a monoclinic $P2_1/c$ structure around 13 GPa. As the monoclinic distortion was negligibly small, our detailed analysis of the high-pressure phase yielded an orthorhombic *Pnma* ($GdFeO_3$-type) structure. The predicted structural parameters for the high-pressure phase at the phase-transition point are given in Table I.

The calculated bulk modulus for the ground-state phase and the possible metastable phases are also given in Table I. The bulk moduli have been obtained using the so-called universal equation of state fit for the total energy as a function of volume. Experimental bulk modulus values are not available for this compound. The calculated bulk modulus for the ground-state and the high-pressure phases are found to be almost double the value of that for the other metastable phases given in Table I and this is associated with the smaller equilibrium volume of the former phases.

The ideal cubic perovskite structure can be considered as a special case of the rhombohedral structure with a rhombohedral angle of 60°. The experimental studies[22,25] show that α_R for $BiFeO_3$ is 59.344°. In contrast, the hitherto available theoretical results[13,19] show that the α_R value is 60.36° for $BiFeO_3$ which can only be achieved by compression of the cubic perovskitelike lattice along the [111] direction. With this background it is interesting to calculate the variation in total energy as a function of the rhombohedral angle for $BiFeO_3$ for the equilibrium volume. The calculated total energy vs α_R given in Fig. 4 clearly show that the theoretical equilibrium rhombohedral angle obtained from accurate total-energy calculation is much smaller than 60° which is consistent with experimental observation. Compared with the total energy corresponding to the earlier theoretically reported[13,19] value for α_R, a gain of 12.9 meV/f.u. is obtained (the total-energy gain from 60° to 59.235° is 6.5 meV/f.u.). Hence our theoretical study confirms the experimental observation that the rhombohedral distortion in the ferroelectric $BiFeO_3$ phase corresponds to an elongation rather than a compression of cubic perovskite-type lattice along [111].

We have also measured high-resolution synchrotron powder-diffraction data collected at the Swiss-Norwegian beam lines at ESRF, Grenoble, for the 2θ range from 3° to 38° and $\lambda = 0.499\,69$ Å. The structural parameters experimentally measured at 115 K are given in Table I and found to be in good agreement with our calculated equilibrium structural parameters for the ferroelectric phase. We also found no significant difference in the measured structural parameters at 115 K for a sample subjected to 0.8 T magnetic field during measurements. More details about the sample preparation and other experimental details will be published later.

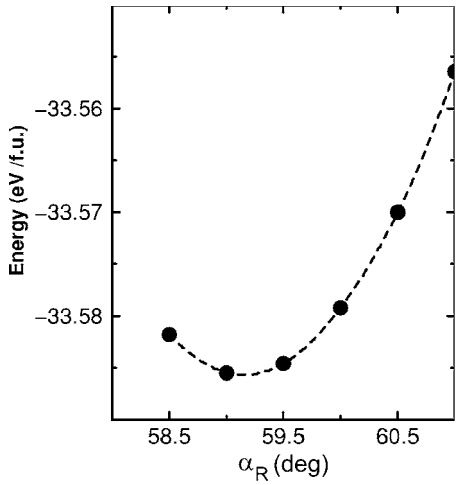

FIG. 4. Total energy as a function of rhombohedral angle (α_R) for $BiFeO_3$ in the ferroelectric *R*3*c* phase.

In order to identify the possible polarization path we mapped the total energy as a function of displacement of Bi ions with respect to the FeO_6 octahedra along [001], [110], and [111] directions in the paraelectric $R\bar{3}c$ phase in Fig. 5. This helps us to visualize the directions of the "easiest" ferroelectric transformation path and to clarify the role of Bi ions on the ferroelectric distortion. The potential-energy surface associated with the displacement of Bi ion along all the three directions [see Fig. 5(a)] are having a double well shape. From Fig. 5 it is clear that the lowest energy off-center displacements are along the [111] directions. This confirms that the polarizability of Bi plays a special role in the ferroelectric properties. The electronic structure studies on $Pb(Zr_{0.5}Ti_{0.5})O_3$ show[60] polarization rotation from the [100] to the [111] direction owing to the smaller energy difference between the tetragonal and the rhombohedral structures. An experimental study[61] on PZT showed that the piezoelectric elongation in tetragonal PZT is along the direction associated with a monoclinic distortion, suggesting the mechanism of polarization rotation via the monoclinic phase. Our total-energy studies on $BiFeO_3$ show that the energy difference between the Bi ion displacement along [111] and [110] directions are relatively small. Consistent with our observation, experimental studies[13] indicate that heteroepitaxially strained thin films of $BiFeO_3$ have tetragonal-like crystal structure with the *c* axis normal to the substrate surface, with a small monoclinic distortion of about 0.5°.

Figure 5 shows that the energy gain associated with the ferroelectric distortion along the [111] direction is 0.427 eV per f.u. This energy gain is found to be much higher than

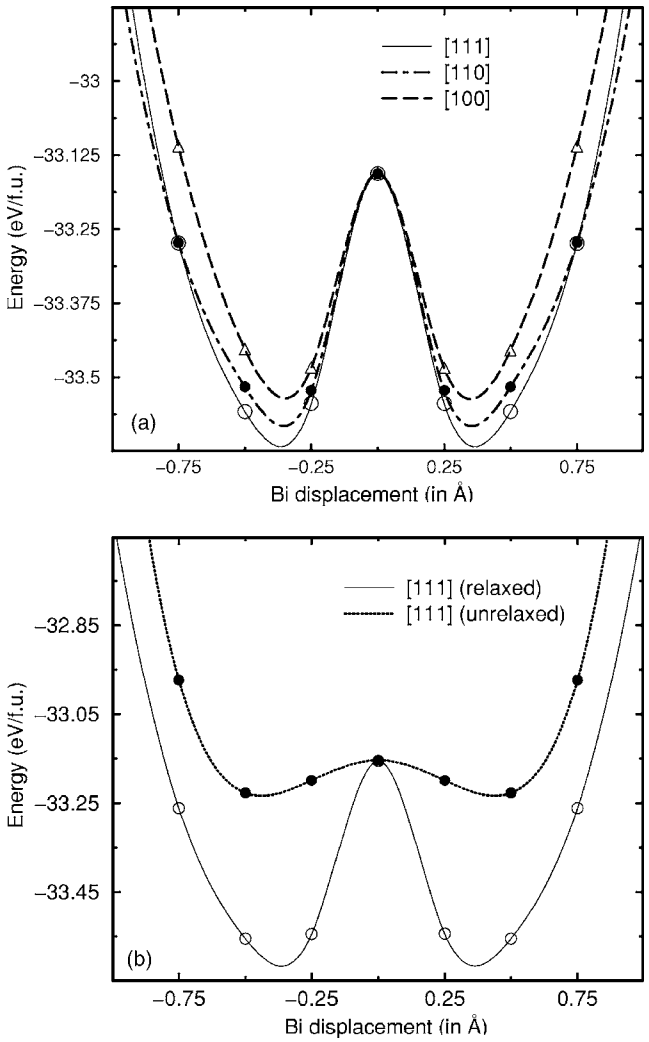

FIG. 5. (a) Total energy as a function of displacement of Bi ion along [100], [110], and [111] directions in the $R3c$ structure for the ferroelectric phase of $BiFeO_3$. (b) The same for $BiFeO_3$ in the [111] direction with or without structural relaxation.

0.056 eV for PZT, the well-known piezoelectric material.[62] It is tempting to try to connect these numbers with the corresponding ferroelectric Curie temperatures. We know that, in principle, the thermal energy required for a system to remain in the high-symmetric paraelectric $R\bar{3}c$ phase will be of the order of energy barrier between these two systems. This suggests that the Curie temperature of $BiFeO_3$ must be much higher than that of PZT. Consistent with this observation the ferroelectric Curie temperature of $BiFeO_3$ is (~1000 K) larger than that of PZT (~570 K). It should be noted that for systems with a competition between different structural instabilities,[63] such an argument can grossly overestimate the transition temperature. In $BiFeO_3$, for example, it is known that there is a competition between the ferroelectric rhombohedral phase (arising from the off-center displacements of ions due to Bi lone pairs) and an antiferrodistortive phase (associated with the lattice mismatch involving rotation of the oxygen octahedra).

B. Chemical bonding

The ferroelectric properties of materials such as $Pb(Zr_{1-x}Ti_x)O_3$ are known to be related to the partial covalency of some bonds.[64,65] In this connection detailed analysis of chemical bonding in $BiFeO_3$ is particularly interesting. Analysis of bonding interaction from charge-density distribution alone may mislead the identification of the nature of chemical bonding correctly.[66] Hence we have used different tools to explore the bonding behavior in $BiFeO_3$. From the analyses of the charge density and densities of states for $PbTiO_3$ and $BaTiO_3$ it is concluded[64,67] that the ferroelectric instability is due to hybridization between the O $2p$ states and the Ti $3d$ states. So, it is interesting to analyze the chemical bonding between Fe and O in $BiFeO_3$ in order to have a better understanding on the origin of ferroelectricity. The electron densities calculated by VASP were shown for a plane containing Bi, Fe, and O atoms in Fig. 6(a). From this figure it is clear that the bonding interaction between Fe and O is not purely ionic. The directional nature of charge density distribution between Fe and O indicates the presence of finite covalent bonding.

Experimental results[68] and detailed theoretical investigations[69] on $BaTiO_3$ showed the significant hybridization interaction between Ba $5p$ and O $2p$ orbitals which contributes to the Born effective charge and ferroelectric properties. In this context, the analysis of the nature of bonding interaction between Bi and O is particularly interesting. The charge-density distribution in Fig. 6(a) shows the presence of finite charges between Bi and O, which is generally an indication for the covalent interaction. Charge-transfer distribution [see Fig. 6(b)] shows that electrons transfer from both Bi and Fe atoms to the oxygen sites consistent with the ionic picture. If one has pure ionic bonding interaction between Bi and O as well as between Fe and O, one would expect an isotropic charge-transfer distribution. The anisotropic distribution of charge transfer confirms the presence of finite covalent bonding between Bi and O as well as between Fe and O.

ELF is an informative tool to distinguish different bonding interactions in solids,[49] here it is shown for ferroelectric $BiFeO_3$ in Fig. 6(c). The negligibly small value of ELF between atoms indicate the presence of dominant ionic bonding in this material. Also the ELF distribution given in Fig. 6(c) shows maximum value at the O sites and minimum value at the Fe and Bi sites reiterate charge-transfer interaction from Bi/Fe to O sites. Moreover, polarization of ELF at the O sites towards the other O sites and finite ELF between Bi and O indicate the hybridization interaction. The conclusion from the charge-density, charge-transfer, and ELF analyses is that the bonding interaction between Bi and O as well as Fe and O are dominant ionic bonding with finite covalent character. This conclusion is consistent with the conclusions arrived from the Born effective charge analysis discussed below. Our results clearly establish the mixed ionic-covalent character of the bonding in $BiFeO_3$: it is obvious that the covalent character is not restricted to the Fe-O bond. It may be noted that while Bi $s-O$ p bonding is not very strong, it is at least as important as the Fe $d-O$ p interaction.

If the bonding between the constituent atoms in $BiFeO_3$ is purely ionic it would remain centrosymmetric (and therefore

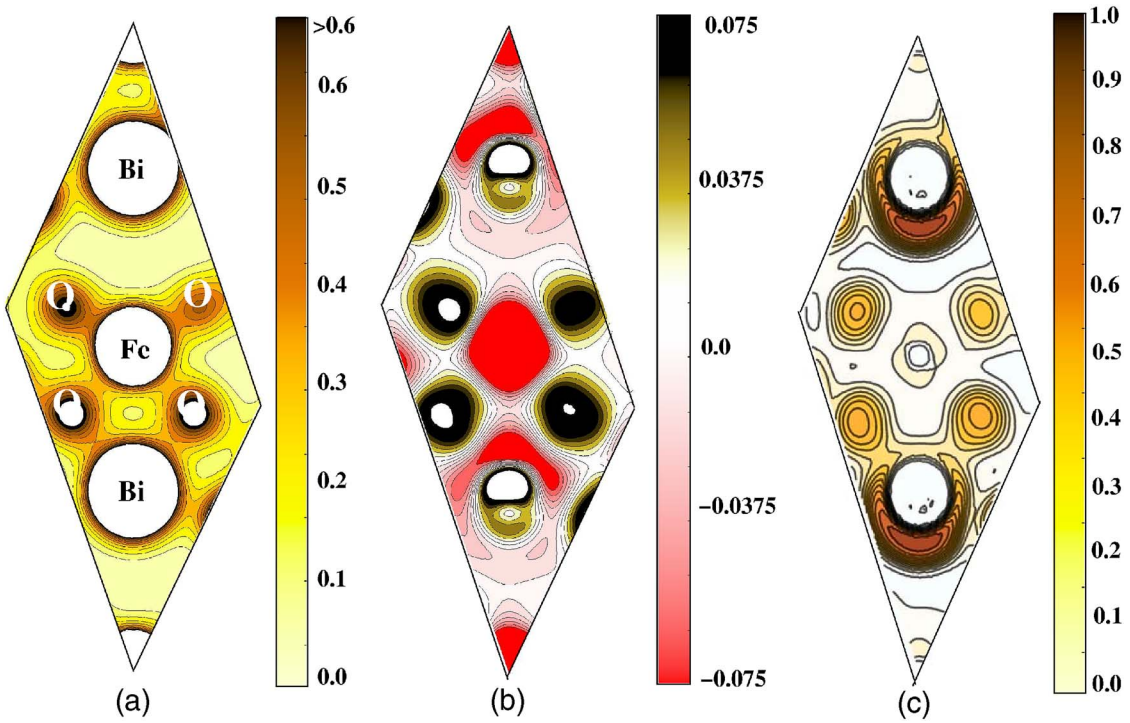

FIG. 6. (Color online) Calculated (a) valence-electron charge density, (b)charge-transfer, and (c) ELF plot for ferroelectric $BiFeO_3$.

not ferroelectric), because the short-range repulsion between adjacent closed-shell ions is minimized for symmetric structures. The existence or absence of ferroelectricity is determined by a balance between these short-range repulsions, which favor the nonferroelectric symmetric structure, and additional bonding considerations which act to stabilize the distortions necessary for the ferroelectric phase. Until now two different chemical mechanisms have been identified for stabilizing the distorted structure in common ferroelectrics. In the first mechanism, the ferroelectric distortion was ascribed to the hybridization interaction between the transition-metal ion and oxygen.[64] The transition-metal ions (such as Ti^{4+}, Zr^{4+}, Nb^{5+}, and Ta^{5+}) participating in hybridization interaction with O are formally in a d^0 state, hence the lowest unoccupied energy levels are d states which tend to hybridize with O $2p$ states.[70] However, this mechanism is not very significant for the case of multiferroics because the transition-metal ions are not in a d^0 state.

The second mechanism involves cations with "lone pair" electrons which have a formal ns^2 valence electron configuration. In the same vein as the d^0 ions discussed above, these p^0 ions (Tl^+, Sn^{2+}, Pb^{2+}, Sb^{3+}, and Bi^{3+}) contain some p charge density which contribute to the displacive distortions. Indeed the tendency of ns^2 ions to lose inversion symmetry is well established, with the conventional explanation invoking a mixing between the localized ns^2 states and a low-lying ns^1np^1 excited state, a mixing that can only occur if the ionic site does not have inversion symmetry.[71] If the lowering in energy associated with the hybridization interaction is larger than the interionic repulsion opposing the ion shift, then a ferroelectric distortion results. This "stereochemical activity of the lone pair" is the driving force for off-center distortion in magnetoelectric materials.

C. COHP

The crystal orbital Hamiltonian population (COHP) is calculated using the tight-binding linear muffin-tin orbital program (TBLMTO).[72] The COHP is the density of states weighted by the corresponding Hamiltonian matrix element and is indicative of the strength and nature of a bonding (negative COHP) or antibonding (positive COHP) interaction.[73,74]

The calculated COHP for the Bi-O, Bi-Fe, and Fe-O interaction for ferroelectric $BiFeO_3$ are shown in Fig. 7. The COHP curves reveal that all occupied states for the Fe-O interaction have bonding states, and the Fermi level is perfectly adjusted to fill up these bonding states. So the strongest bonding interaction is between Fe and O atoms. The FeO_6 octahedra are highly distorted and hence the Fe-O2 bonding energy (−1.52 eV) is stronger than the Fe-O1 interaction (−1.02 eV) where O1 and O2 are planar and apical oxygen atoms, respectively. Considerable amount of bonding states within the valence band (VB) in COHP shows significant bonding interaction between Bi and O atoms. It should be noted that a large bonding-state peak appearing around −10 eV (between the Bi-O interaction) is due to the hybridization interaction between the Bi $6s/6p$ and O $2s$ states. As the COHP is estimated from TBLMTO method, we found a shift in the density of states (DOS) value by around 1 eV towards higher energy with respect to that from VASP. From the COHP analysis it is clear that the hybridization interaction between Bi/Fe and O is significant, and it is an important driving force for the ferroelectric distortion. The COHP for Bi-Fe interaction shown in Fig. 7 indicates the presence of both bonding and antibonding states within the VB. However, the bonding interaction between Bi and Fe in $BiFeO_3$ is

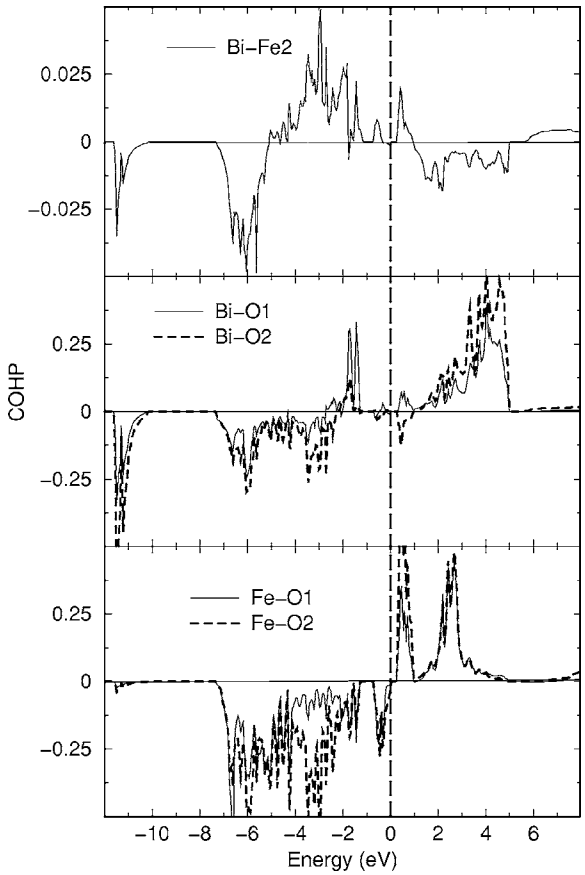

FIG. 7. COHP for $BiFeO_3$ in the ferroelectric $R3c$ structure describing Bi-O, Fe-O, and Bi-Fe interactions. O1 and O2 are the planar and apical oxygen atoms, respectively.

weaker than that between all the other atoms.

D. Band structure results

In order to gain more insight into the role of ferroelectric distortion on electronic structure and bonding behavior in $BiFeO_3$, the calculated band structure for A-AF phase of $BiFeO_3$ in the paraelectric $R\bar{3}c$ structure and the ferroelectric $R3c$ structure are given in Figs. 8(a) and 8(b), respectively. As in the $R\bar{3}c$ phase [Fig. 8(a)], the highest-energy valence states have noticeable O $2p$ character and the lowest conduction-band states are Bi $6p$-like, at variance with the Ti $3d$ bands in $PbTiO_3$. This together with the relatively narrow band gap of the paraelectric $R\bar{3}c$ phase results in ferroelectric instabilities mainly characterized by a hybridization between Bi $6p$ and O $2p$ orbitals, not the one involving d bands of the transition-metal cation that is typical of most other ferroelectric perovskites.[65,75] It is interesting to note that the highest energy valence-band state of $R3c$ phase has dominant Fe $3d$ states and these states are shifted to around 0.35 eV to the lower energy in the paraelectric phase. In the $R3c$ phase [see Fig. 8(b)] the gap opens considerably and the top valence bands increase their Bi $6p$ character (see also Fig. 9). The strong Bi $6p$–O $2p$ hybridization is also reflected in the fact that the effective charge on Bi in the ferroelectric $R3c$ phase has a larger value than that in the paraelectric $R\bar{3}c$ phase (see Sec. III G).

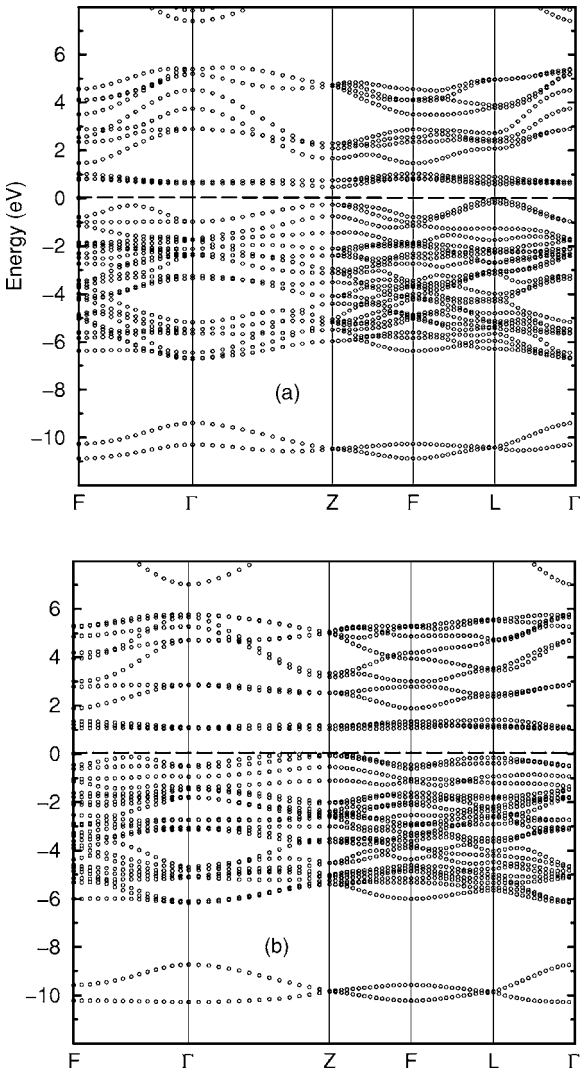

FIG. 8. Electronic band dispersion for antiferromagnetic $BiFeO_3$ in (a) paraelectric $R\bar{3}c$ and (b) ferroelectric $R3c$ structures. The Fermi level is set to zero.

Two well dispersed bands around −10 eV are mainly originating from Bi−6s electrons. Compared with the paraelectric phase, these two bands are slightly broader in the ferroelectric phase. The O $2s$ bands are completely filled and they are located around −18 eV below the Fermi level and are not shown in Figs. 8(a) and 8(b). The parabolic nature of bands around −6 eV are from Fe $4s$ electrons with significant contribution from both O $2p$ and Fe $3d$ electrons. A series of bands between −6 eV and the Fermi level are mainly originating from hybridized bands of both Fe $3d$ and O $2p$ electrons.

Owing to the off-center displacement of the ions in the ferroelectric phase of $BiFeO_3$, the degeneracy in bands along the F-Γ direction in Fig. 8(b) are lifted compared to that of paraelectric phase. When the system is allowed to relax to its magnetic ground state a gap opens and an insulator is formed, as required for the ferroelectric state. The ferroelectric distortion slightly increases the band-gap values, from

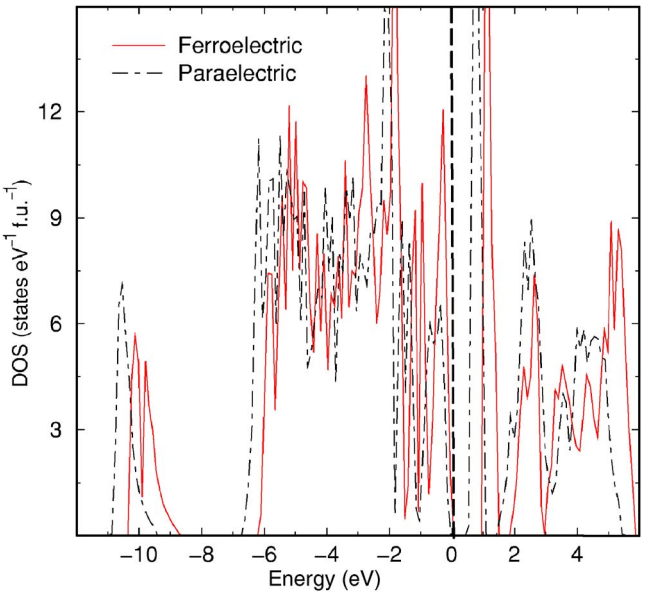

FIG. 9. (Color online) Calculated total density of states for $BiFeO_3$ in the paraelectric $R\bar{3}c$ and ferroelectric $R3c$ phases.

0.46 eV in the paraelectric to 0.97 eV in the ferroelectric phases. The density functional calculations are known to underestimate the band gap and hence the reported values will be smaller than the real band-gap value for this material. The Bi ions are almost in the 3+ ionic state and hence the contribution from Bi $6p$ electrons are relatively small in the VB and they are mainly in the CB around 2–6 eV.

In order to understand the sensitivity of electronic structure by ferroelectric displacement, the calculated total density of states for the paraelectric and the ferroelectric phases of $BiFeO_3$ are superimposed in Fig. 9. From this figure it is clear that overall energy of electrons in the ferroelectric phase is shifted around 0.5 eV from the paraelectric phase due to the off-center displacement of ions. This also highlights the different bonding interaction between planar oxygen and Fe due to the buckling of the FeO_6 octahedra to accommodate the Bi $6s^2$ lone pair electrons occurring after the phase transition. In fact, the changes in the ferroelectric phase found at the top of the VB involve the d_{z^2} states of Fe and the p_z states of the apical oxygen, whose stronger hybridization gives more stability to the structure in the ferroelectric phase.

To simplify the interpretation of the electronic structure, we have also calculated the partial (atom and orbital decomposed) densities of states for the ferroelectric $BiFeO_3$ (see Fig. 10). The top of VB is set to zero. Around −18 eV the lowest energy VB states form a filled, rather narrow band from O $2p$ electrons. Above these states (around −10 eV) lone pair Bi $6s$ states with small contribution from O $2s$ and $2p$ electrons are present. The Fe $4s$ states are located around −6 eV in the VB and they are completely mixed with the Fe $3d$ states in the entire VB. The energetically degenerate nature of Fe $3d$ and O $2p$ in the whole VB indicates the presence of covalent bonding between these two atoms. Bi $6s$ and $6p$ states are well separated and the latter states are mostly in the CB implying highly ionic nature of Bi ions.

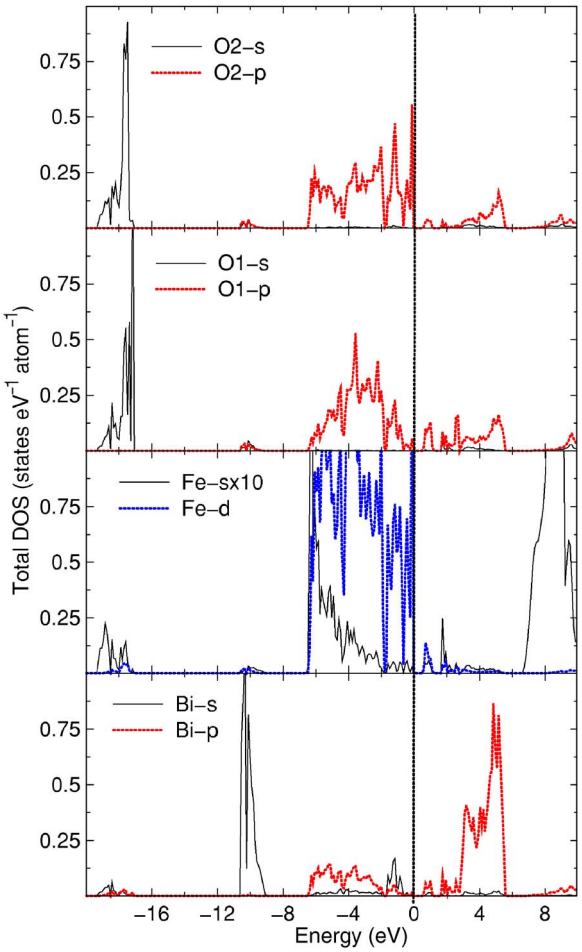

FIG. 10. (Color online) Partial density of states for ferroelectric $BiFeO_3$ in the G-AF state.

E. Magnetic properties

Crystalline $BiFeO_3$ is a strong antiferromagnet (G-type spin structure, T_N=654.9 K).[76] The cooperative magnetism in $BiFeO_3$ is originating from the half filled and localized ($t_{2g}^3 e_g^2$) Fe^{3+} ions. In an ideal cubic perovskitelike lattice, the Fe^{3+} ions in the high spin state prefer to form the G-AF ordering because in this case the Pauli exclusion principle allows the transfer of electron to the neighboring ion in an antiparallel direction only. The neutron-diffraction studies carried out at room temperature revealed that $BiFeO_3$, in fact, exhibits a compensated antiferromagnetic ordering (T_N=670 K), with a cycloidal spin arrangement, incommensurate with its lattice.[77] The magnetic structure of a separate unit cell corresponds to the G-type antiferromagnetic ordering (each magnetic Fe^{3+} ion is surrounded by six Fe^{3+} ions with spins directed opposite to that of the central ion).[47] Indirect evidence of the existence of the spatially spin-modulated structure (SSMS) in $BiFeO_3$ was obtained[12] from the measurements of the magnetoelectric effect. The existence of SSMS with periodicity of 620 Å was recently confirmed by ^{57}Fe NMR measurements.[78]

Dzyaloshinskii[9] developed a thermodynamic theory based on spin-lattice interaction and magnetic dipole interaction to explain the origin of weak ferromagnetism in antiferromag-

TABLE II. Total energy (relative to the lowest energy state in meV/f.u.), Fe-magnetic moment (in μ_B/atom), and total magnetic moment (including those at oxygen and interstitial sites; μ_B/f.u.) for $BiFeO_3$ in *A*-, *C*-, *G*-AF, and F states in the ferroelectric *R*3*c* structure.

	A-AF	*C*-AF	*G*-AF	F
Energy	0	211	171	390
Fe-magnetic moment	3.724	3.824	3.789	3.936
Total magnetic moment	3.885	3.974	4.076	4.893

netic compounds. The basic assumption is that antiferromagnetically ordered spins could rotate about a crystal axis toward one another, resulting in a net spontaneous moment over the unit cell. The calculated magnetic moments and the total energy with respect to the ground-state magnetic configuration for $BiFeO_3$ are given in Table II. It is interesting to note that the energy difference between the ferromagnetic state and different antiferromagnetic state is larger compared with that for $LaMnO_3$ (in $LaMnO_3$ the energy difference between the ferromagnetic and the *A*-AF state is only 25 meV/f.u.).[79] This observation is consistent with the experimental measurements in the sense that amorphous phase of $BiFeO_3$ is found to be in a speromagnetic state (short-range antiferromagnetic behavior) rather than in a ferromagnetic state.[80]

Like $LaFeO_3$, $BiFeO_3$ also has Fe ions in the 3+ states. Similar to $LaFeO_3$ one could expect *G*-AF ordering in $BiFeO_3$. But, owing to the presence of lone pair electrons at the Bi sites, one could expect anisotropy in the exchange interaction also. Consistent with this expectation we found that the *A*-AF state is found to be 171 meV/f.u. lower in energy than the *G*-AF state in $BiFeO_3$. This suggests that the Bi lone pair electrons play an important role in not only the ferroelectric behaviors but also in the magnetic properties of $BiFeO_3$. The observation of *A*-AF ordering is particularly interesting. In $LaMnO_3$ each MnO_6 octahedron is elongated along one axis as a result of the Jahn-Teller distortion around the d^4 Mn ions. This Jahn-Teller distortion creates orbital ordering that leads to four singly occupied d_z^2 orbitals pointing towards empty $d_{x^2-y^2}$ orbitals on adjacent Mn ions (a ferromagnetic interaction) and two empty $d_{x^2-y^2}$ orbitals pointing towards other empty $d_{x^2-y^2}$ orbitals (an antiferromagnetic interaction) resulting in the *A*-AF ordering.[79] If no other mechanism was involved in the stabilization of magnetic ordering in $BiFeO_3$ one could expect *G*-AF ordering as that in $LaFeO_3$. But, owing to the Bi lone pair electrons, we found *A*-AF phase to be the ground state for $BiFeO_3$ among the considered collinear magnetic configurations. It should be noted that if the Coulomb correlation effects are important in this material, one could expect that the energetics of different magnetic configurations will be different from the values reported here. But, as most of the features of magnetoelectric behavior of $BiFeO_3$ are well described by GGA itself, we have not considered Coulomb correlation effects in the present study.

The calculated magnetic moment at the Fe site varies between $3.724\mu_B$ and $3.936\mu_B$ per Fe atom depending upon the magnetic configuration considered in our calculations (see Table II). The calculated magnetic moment at the Fe site is found to be in good agreement with the value of $3.75(2)\mu_B$ measured from low-temperature neutron-diffraction measurements.[25] The calculated magnetic moments at the iron sites are not integer values, since the Fe electrons have a hybridization interaction with the neighboring O ions. Because of this hybridization interaction we found that around $0.18\mu_B$ magnetic moment is induced at each O site in the ferromagnetic state which are polarized along the same direction as that in the Fe sites. As a result the net total moment at the site is considerably larger (see the total moment in Table II).

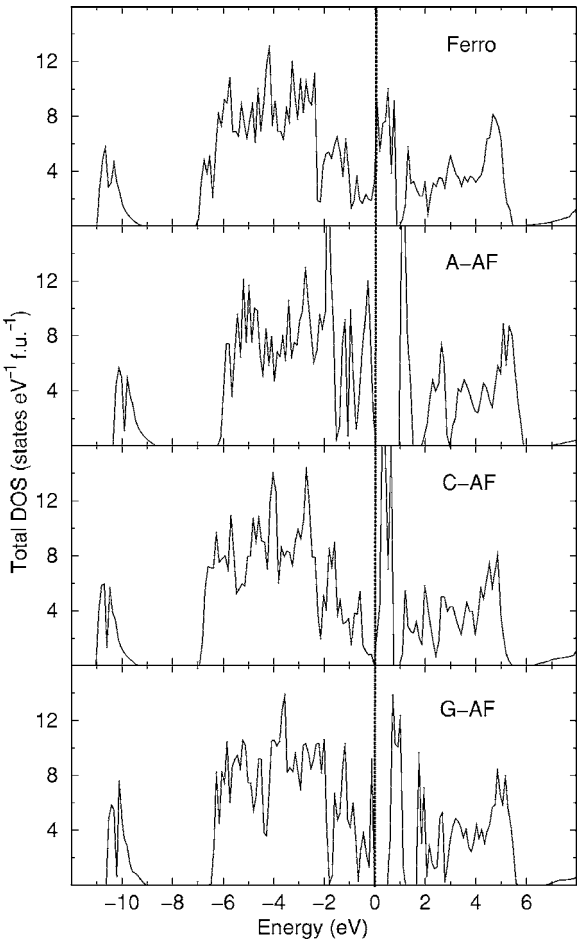

FIG. 11. Calculated total density of states for $BiFeO_3$ in different magnetic configurations. The Fermi level is set to zero.

The calculated total DOS for $BiFeO_3$ in the nonmagnetic and ferromagnetic states show metallic behavior with a large DOS at the Fermi level. The large number of electrons near the Fermi level is not a favorable condition for stability. However, when one creates AF ordering, the exchange interaction produces an exchange potential that effectively shifts the energy of the Fe 3*d* band to lower energy giving insulating behavior as shown in Fig. 11. We found that even if we introduce spin polarization into the calculation, the electronic ground state depends upon the nature of magnetic ordering. The Fermi level lies in a pseudogap feature in the *C*-AF state and clear insulating behavior is observed for the *A*-AF and

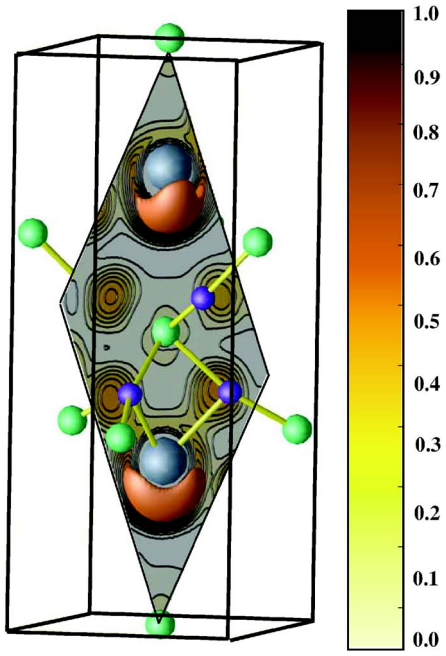

FIG. 12. (Color online) Isosurface (at a value of 0.75) of the valence electron localization function of $BiFeO_3$ in the ferroelectric $R3c$ structure obtained from TBLMTO calculation. The atom labels in the shown plane are same as that in Fig. 6(a).

G-AF ordered states with band gaps of 0.97 and 0.53 eV, respectively. If the correlation effects are not significant in this material, the present result suggest that magnetic ordering plays an important role in stabilization of ferroelectricity. However, it should be noted that the magnetic ordering temperature is much smaller (643 K) than the ferroelectric ordering temperature (1100 K). Hence it appears that mechanisms other than magnetism may establish insulating behavior and ferroelectricity at high temperatures.

F. Role of Bi lone pair electrons for ferroelectricity

The ELF provides a measure for the local influence of the Pauli repulsion on the behavior of electrons and permits the mapping in real space of core, bonding, lone pair, and nonbonding regions in a crystal.[81] We have used the TBLMTO program to calculate the ELF. In order to visualize the lone pairs around Bi, it was necessary to select an isosurface with an ELF value of 0.75 as shown in Fig. 12. This figure reveals the lobelike lone pairs possessed by the Bi atoms. It also indicates that the Bi 6*s* orbitals are in direct interaction with oxygen 2*p* and are thus not chemically inert. An interesting feature of ELF for $BiFeO_3$ in Fig. 6(c) is the presence of a nonuniform distribution of ELF at the Bi sites. The reason for this is that due to the displacement of the Bi atoms, the Bi $6p_z$ orbital can interact more efficiently with the O $2p_x$ and O $2p_y$ orbitals. In the $R\bar{3}c$ structure, these orbitals interact only with the Bi 6*s* orbitals because the symmetry does not allow for an interaction with the Bi $6p_z$ orbitals. In the $R3c$ structure, half of the Bi atoms have moved in the $+z$ direction and another half of them in the $-z$ direction, breaking the symmetry and allowing hybridization between the indicated linear combination of O orbitals and the Bi p_z orbital. As a result, some of the O p_x/O p_y derived states (in fact, those that had the strongest interaction with the Bi 6*s* state) are lowered in energy and move away from the Fermi surface, effectively counterbalancing the destabilization caused by the Bi lone pair. The combination of large values of ELF and the covalency leads to a stronger lone pair, which is more stereochemically active. The manner in which the lone pairs dispose themselves suggests a greater tendency to the ferroelectric distortion.

The lone pairs are expected to have primarily 6*s* character. If they are to form lobes, there must be some hybridization interaction with the neighbors. The question is whether the *p* character arises from mixing *s* and *p* states on the Bi atom or is it an effect of covalency, arising from Bi *s* and O *s*/*p* mixing. The partial DOS analysis (see Fig. 10) shows that Bi 6*s* electrons are around −10 eV below the Fermi level and are well localized. Also the Bi-*s* and *p* states are well separated indicating that the mixing between *s* and *p* on the Bi site is minimal. Watson and Parker[82] have recently suggested that it is due to *p* character from the anions that lone pairs are allowed to form lobe-shaped structures. The anion is clearly implicated since in a homologous series of compounds, changing the anion often greatly affects the stereochemistry of the lone pair.[83] If the lone pair 6*s* electrons overlap with the O *s*/*p* states it can attain the typical lobe shape, conversely, in a situation where there is no such overlap, or when the overlap is weak, the lone pair could retain its pure 6*s* character and remain spherical.

In $BiFeO_3$ the charge density and ELF analysis (see Fig. 6) show noticeable covalent bonding between Bi and O. In order to have covalent bonding between Bi *s* and O *p* states they should be energetically degenerate. On the other hand the O *p* states are mainly present at the top of the VB. Although both Bi *s* and O *s* states are well localized and energetically well separated, they are spatially well dispersed. Owing to the spherically symmetric nature of the *s* orbitals, the probability of the hybridization interaction between *s* orbitals is much larger than that between any other orbitals. Hence the lobe shape of the lone pair is at least partly associated with the hybridization interaction between Bi *s* and O *s* states. Even though O *p* states are mainly present at the top of the valence band, finite O *p* electrons are present around −10 eV where the Bi 6*s* electrons are also present. So, both O *s* and *p* electrons participate in the hybridization interaction with the Bi 6*s* electrons. Consistent with this viewpoint our COHP analysis (see Fig. 7) indicates that Bi-O bonding states are present around −10 eV.

It was argued by Orgel,[84] and has been assumed in much of the literature, that the interaction between occupied cation *s* and unoccupied cation *p* bands is the primary cause for the lobe formation. The partial DOS analysis clearly shows (see Fig. 10) that Bi *s* and *p* states are well separated. Hence our observation does not support this classical view of hybridization of the Bi 6*s* and 6*p* orbitals. Rather, it supports the observation of hybridization interaction between the anion *s* and cation *p* states as seen in PbO and related compounds.[82,83] The formation of the distorted electron densities and crystal structures will thus depend on the energies of the valence orbitals of oxygen ions involved in bonding to Bi.

Although the *s* states of both Bi and O are well below the VB their importance for ferroelectric distortion can be understood as follows. The *s* states are spherically symmetric and diffuse compared to the *p* or *d* states. Hence the overlap interaction between *s* states will be stronger than that between other states. Owing to the highly ionic nature of Bi, the Bi 6*p* states are mostly in the unoccupied state (see Fig. 10) but with some noticeable Bi 6*p* states also at the VB. It has been shown that the stereochemical activity of the cation lone pair is determined by the interaction of cation *s* and *p* states with anion *p* states.[85] Hence the activity of the lone pair will be stronger if the covalent interaction between Bi and O is larger, where it has the stereochemical effect of stabilizing the distorted low symmetric structures. Stability of a distorted structure depends on whether the energy gained from hybridization interaction (bonding) between occupied and unoccupied states compensates the energy required to promote an electron to unoccupied state. Since the same oxygen *p* states are involved in both interactions and hence in instabilities, a competition results.

$BiFeO_3$ belongs to the ferroelectrics of displacive type. Now we try to understand the role of lone pair on the ferroelectric behavior. The lone pair occupies as much volume as an oxide or fluoride anion in crystals.[86] The $6s^2$ electrons of Bi^{3+} hybridize with 2*s* and 2*p* of oxygen to form a space-filling localized lobe, which in turn pushes away its neighboring atoms causing a structural distortion. The presence of lone pair makes the hybridization interaction between Bi and O different in different directions. Moreover, the effective ionic radius of Bi ions decreases on one side and increases on the other side. The anisotropic nature of electrons at the Bi sites (originating from the presence of lone pair) stabilizes off-center displaced structure. This results in the movement of the Bi ion in the [111] direction which causes a cooperative displacement of the Fe^{3+} ions due to the repulsive interaction and finally gives rise to a ferroelectric polarization.

G. Born effective charge analysis

The Born effective charge (BEC) Z^* is a fundamental quantity for the study of lattice dynamics, because it governs the amplitude of the long-range Coulomb interaction between nuclei, and the splitting between longitudinal optic (LO) and transverse optic (TO) phonon modes. In binary crystals,[87] infrared measurements of the splitting between LO and TO modes allow an accurate estimation of $\|Z^*\|^2/\epsilon_\infty$ and offer therefore an unambiguous way to extract the amplitude of Z^* from the experiment. But, in complex compounds like perovskite oxides, LO and TO mode eigenvectors are not necessarily equivalent and the determination of Z^* from the experimental data is consequently not straightforward.[88] Hence the development of theoretical methods giving direct access to Z^* acquires specific interest.

The dynamical charge measures the macroscopic current flowing across the sample while the ions are adiabatically displaced. Such currents are responsible for building up the spontaneous polarization, when ions are continuously displaced from the centrosymmetric structure to the ferroelectric structure.[26,27] These displacements are directly observable when measuring polarization via hysteresis cycles. The modern theory of macroscopic polarization[89] allows the calculation of such currents as Berry phases. The dynamical Born effective-charge tensor Z^* of a given ion measures (by definition) total macroscopic current adiabatically transported by the ion moving with unit velocity, while all the other ions and the macroscopic field are kept fixed.[90]

According to the modern theory of polarization,[26,89,91] the change in macroscopic polarization between two different insulating states can be regarded as a measure of the phase difference between their initial and final many-body wave functions. The total polarization **P** for a given crystalline geometry can be calculated as the sum of ionic and electronic contributions.

The ionic contribution is obtained by summing the product of the position of each ion in the unit cell with the nominal charge of its rigid ion core. The electronic contribution to **P** is determined by evaluating the phase of the product of overlaps between cell-periodic Bloch functions along a densely sampled string of neighboring points in **k** space.

It has been shown[92,93] that the effective-charge tensors are almost constant along the path connecting the two structures, which implies that the spontaneous polarization is simply expressed in terms of the internal-strain displacement u_τ as

$$\mathbf{P}_\tau = \frac{|e|}{\Omega}\Sigma_\tau Z_\tau^* u_\tau, \tag{2}$$

where Ω is the cell volume, and Z_τ^* are the diagonal components of the effective-charge tensors for atom τ. BEC can be defined as a linear term in the polarization change due to a unit displacement of the τth ion, keeping all the other ions fixed under the condition of zero macroscopic field,[90] i.e.,

$$Z_{\tau\alpha\beta}^* = \Omega \left.\frac{\Delta \mathbf{P}_\beta}{\Delta u_{\tau\alpha}}\right|_{\epsilon=0} \tag{3}$$

for the change in **P** on moving ion τ; note that the effective charge is a tensor. Thus the effective charge is calculated by finding the induced polarization of the nuclei and the electrons when the nuclei are displaced equally in each unit cell, so that the translational periodicity is the same as the undistorted crystal. The effective charge thus found is the transverse Born effective charge[94,95] since the macroscopic electric field is required to vanish. According to the modern theory of polarization,[26,89] the total difference in polarization between a reference state and a state where the atoms belonging to the sublattice τ have been displaced by a small but finite distance $\Delta u_{\tau\alpha}$ is defined as

$$\Delta \mathbf{P} = \Delta \mathbf{P}_{el} + \Delta \mathbf{P}_{ion} \tag{4}$$

where $\Delta \mathbf{P}_{el}$ is the electronic contribution obtained from the Berry-phase polarization approach and $\Delta \mathbf{P}_{ion}$ is the ionic contribution. $\Delta \mathbf{P}_{ion}$ is defined by

$$\Delta \mathbf{P}_{ion} = \frac{|e| z_\tau \Delta u}{\Omega}, \tag{5}$$

where z_τ is the valence atomic number of the τth atom. For practical purposes, the electronic contribution to Z^* can be obtained as

TABLE III. Calculated Born effective charge tensor for antiferromagnetic $BiFeO_3$ in the paraelectric $R\bar{3}c$ and ferroelectric $R3c$ structures.

Z^*	Position	xx	yy	zz	xy	xz	yx	yz	zx	zy
$R\bar{3}c$										
Bi	(1*a*)	5.048	4.975	4.243	0.104	−0.058	−0.081	−0.058	−0.001	0.000
Bi	(1*a*)	5.048	5.071	4.240	−0.105	−0.058	0.0330	−0.058	0.000	0.000
Fe	(1*a*)	4.537	4.607	3.205	−0.185	−0.069	0.2170	−0.072	0.000	0.000
Fe	(1*a*)	4.537	4.568	3.207	0.186	−0.068	−0.115	−0.067	0.000	0.000
O	(3*b*)	−3.799	−2.601	−2.583	0.149	0.265	−0.038	0.629	0.211	0.608
O	(3*b*)	−2.978	−3.469	−2.584	0.418	0.434	0.636	0.554	0.421	0.486
$R3c$										
Bi	(1*a*)	5.438	5.460	4.792	−0.022	−0.004	−0.001	0.004	0.000	0.000
Bi	(1*a*)	5.434	5.414	4.791	0.022	0.005	0.001	−0.005	−0.001	0.000
Fe	(1*a*)	5.224	5.223	4.859	−0.777	−0.001	0.777	0.000	0.000	0.000
Fe	(1*a*)	5.224	5.222	4.858	0.777	0.000	−0.777	0.000	0.000	0.000
O	(3*b*)	−3.590	−3.496	−3.227	−0.048	0.409	0.000	0.000	0.530	−0.023
O	(3*b*)	−3.551	−3.533	−3.226	−0.062	−0.212	−0.032	−0.347	−0.285	−0.446

$$Z^{el}_{\tau\alpha\beta} = \Omega \lim_{\Delta u_{\tau\alpha}\to 0} \frac{\Delta \mathbf{P}_e}{\Delta u_{\tau\alpha}}. \tag{6}$$

In periodic systems, the change in electronic polarization in zero field can be computed from the King-Smith and Vanderbilt formula:[26]

$$\mathbf{P}^{el}_{\beta} = -\frac{1}{(2\pi)^3} i\Sigma_n^{occ} s \int_{BZ} \langle u_{nk}|/\partial/\partial k_\beta|u_{nk}\rangle dk, \tag{7}$$

where s is the occupation number of the valence-band states ($s=1$ for the spin-polarized case) and u_{nk} are the periodic parts of the Bloch functions. This definition is valid only under the constrain that the wave functions fulfill the periodic gauge condition. This means that the periodic parts of the Bloch functions must satisfy

$$u_{nk}(r) = e^{i\mathbf{G}\cdot\mathbf{r}} u_{nk+\mathbf{G}(\mathbf{r})}. \tag{8}$$

Once $\Delta\mathbf{P}$ is known, the Born effective charge tensor for the β component can be obtained from the formula (3) where α denotes the direction of polarization. For a continuous change, such as the induced polarization when atoms are displaced, uncertainties by possible integral multiples of 2π can be avoided by defining small enough changes where one always knows that the change in polarization is given by the smallest value, i.e., with the integer equal zero. Hence in the Berry-phase calculations, we have chosen the displacement of 0.03 Å, and used a set of strings of eight **k** points (parallel to some chosen reciprocal-lattice vectors) to calculate the electronic polarization. Our results shown in Table III satisfy the acoustic sum rule, $\Sigma_k Z^*_{k,ii}=0$, indicating that the calculations are well converged with respect to computational conditions.

Our calculated zz component of the BEC can directly be compared with the BEC values given in Table IV in Ref. 19. The formal valence of Bi, Fe, and O in $BiFeO_3$ are 3+, 3+, and 2−, respectively. In simple, high-symmetry oxides, the oxygen Z^* is isotropic and is close to −2.[96] However, simple models[97] hint at nontrivial values of Z^*. When we include AF ordering into the calculations, because of the loss of symmetry, the space group changed from $R3c$ to $R3$. Owing to the site symmetry, the diagonal components of Z^* are anisotropic for all the ions in Table III. If ions have closed-shell-like character, each ion will carry an effective charge close to their nominal ionic value according to a rigid-ion picture. On the contrary, a large amount of nonrigid delocalized charge flows across this compound during the displacement of ions owing to the covalence effect.[65,93] Consequently, we have obtained effective charges much larger than the nominal ionic value. The charges on Bi, Fe, and O are around 75% larger than they would have been in a pure ionic picture: this reveals the presence of a large dynamic contribution superimposed to the static charge. Similar giant values of Z^* have been reported using quite different technical ingredients and/or for other perovskite oxides.[69,93]

The BEC is indeed a macroscopic concept,[90,98] involving the polarization of valence electrons as a whole, while the charge "belonging" to a given ion is an ill-defined concept. The high BEC values indicate that relative displacements of neighboring ions against each other trigger high polarization. Roughly speaking, a large amount of nonrigid, delocalized charge is responsible for higher value of BEC than the nominal charges. The calculated BEC for the ferroelectric and the paraelectric phases are given in Table III. It is clear that both Bi and Fe donate electrons and O accepts electrons, consistent with the traditional ionic picture. It can be recalled that for a pure ionic system one could expect more isotropic value for Born effective charges. Considerable anisotropy in the diagonal components of BEC given in Table III and the noticeable off-diagonal components in the oxygen sites confirm the presence of covalent bonding between O $2p$ and Fe $3d$ orbitals. It is generally expected that there is considerable covalent bonding between Fe and O within the FeO_6 octahedra and this could explain the presence of anomalous contri-

butions (defined as the additional charge with respect to the well-known ionic value) to the effective charge at the Fe and O sites. Surprisingly large anomalous charge at the Bi site (+1.8 to +2.4) gives tangible proof for hybridization interaction between Bi and the neighboring O atoms. When going from the paraelectric phase to the ferroelectric phase, we have observed considerable increase in the effective charges in all three constituents. This is associated with the anisotropy in the chemical environment. While FeO_6 octahedra are equally distanced from Bi ions in the paraelectric phase, a short and a long Bi-FeO_6 distance arise in the ferroelectric phase owing to the off-center displacement of the Bi ions.

H. Spontaneous polarization

One of the basic quantities of ferroelectrics is spontaneous macroscopic polarization **P**, which results upon application of an electric field, and persists at zero field in two (or more) enantiomorphous metastable states of the crystal. Experiments measure **P** via hysteresis cycles from the difference $\Delta\mathbf{P}$ between these metastable states.[99] Even though $BiFeO_3$ has large atomic displacements relative to the centrosymmetric cubic perovskite structure, and the high ferroelectric Curie temperature (1100 K), early measurements yielded rather small polarizations.[17,23,24] The small values are in sharp contrast to the experimental findings on epitaxial thin films[13,16,100] which were found to possess large polarizations. There are several plausible explanations given for the large difference in values of polarization reported experimentally. One possibility is that the original reports of small polarization might have been limited by poor sample quality.[17] A second possibility is that the small values could be correct for the $R3c$ structure, with the large values being correct for different structural modifications stabilized in the thin films.[13] Recently the large and small values are explained within the modern theory of polarization, which recognized that polarization is in fact a lattice of values, rather than a single vector.[19] Hence it is interesting to analyze the spontaneous polarization present in $BiFeO_3$ in detail with the help of accurate density functional calculations.

We calculated the polarization difference $\Delta\mathbf{P}$ between the polar $(R3c;\lambda=1)$ and the ideal $(R\bar{3}c;\lambda=0)$ rhombohedral structures assuming a continuous adiabatic transformation which consists of scaling the internal strain with the parameter λ $(0\leqslant\lambda\leqslant u)$. The polarization at the paraelectric $R\bar{3}c$ phase $[\mathbf{P}(\mathbf{0})]$ would be zero (since there is no dipole for this case) and would be a finite value $\mathbf{P}(\mathbf{u})$ for the ferroelectric $R3c$ phase. The dipole moment evolves continuously from $\mathbf{P}(\mathbf{0})=0$ to $\mathbf{P}(\mathbf{u})$, i.e.,

$$\int_0^u Z^*(u)du = [\mathbf{P}(u) - \mathbf{P}(0)] = uZ(u), \tag{9}$$

where

$$Z(u) = \frac{1}{u}\int_0^u Z^*(u)du. \tag{10}$$

The mean value of $Z^*(u)$ from 0 to u is equal to $Z(u)$. We have calculated the polarization along x, y, and z directions using three different approximations in Table IV, i.e., by assuming (i) the $Z(u)$ values same as $Z^*(u)$ values of ferroelectric phase, (ii) the $Z(u)$ values are same as $Z^*(u)$ values of paraelectric phase, and (iii) the $Z(u)$ values is an average of $Z^*(u)$ value of the ferro-, and paraelectric phases. The Z^*_{zz} eigenvalues of Bi and Fe correspond to an eigenvector aligned along the ferroelectric axis. Hence the calculated polarization values corresponding to $\mathbf{P}_z$ obtained from (iii) can be directly compared with the experimentally measured values.

TABLE IV. Cartesian components of the polarization $\Delta\mathbf{P}_\alpha$ for $BiFeO_3$ calculated using Eq. (2) along a path from the paraelectric $R\bar{3}c$ phase to the ferroelectric $R3c$ phase. The polarization values (in $\mu C/cm^2$) calculated with the Born effective charges for $R\bar{3}c$, $R3c$ structures and the average value for these two structures (noted by "average").

Z^* values used in Eq. (2)	$\mathbf{P}_x$	$\mathbf{P}_y$	$\mathbf{P}_z$
$R\bar{3}c$	−0.02	−0.01	93.85
$R3c$	1.33	2.85	83.53
Average	0.65	1.41	88.69
Point charge	0	0	60.19

The $R3c$ symmetry permits the development of a spontaneous polarization along [111], and Bi, Fe, and O are displaced relative to one another along this threefold axis. In the case of O, the eigenvector associated with the highest eigenvalue is positioned approximately along the direction of Fe-O bond. We identify that the highest contribution originates from the equatorial plane of the FeO_6 octahedron. The largest relative displacements are those of Bi relative to O owing to the presence of stereochemically active Bi lone pair.[101] The off-center displacements are noticeably larger compared to those in non-lone-pair-active perovskite ferroelectrics such as $BaTiO_3$ or $LiNbO_3$,[64,102] but are consistent with those observed in other Bi-based perovskites.[62]

Our partial polarization analysis shows that the polarization contribution coming from Bi, Fe, and O atoms are 86.94, 18.91, and −17.15 $\mu C/cm^2$, respectively, along [111] direction. This indicates that the polarization contribution arising from displacement of Fe and O atoms are almost canceling out and more than 98% of the net polarization present in $BiFeO_3$ is contributed by the Bi ions. The oxygen ions are displaced in the same direction as Bi and Fe. However, the negative value of Born effective charges at the oxygen sites is responsible for the opposite direction of polarization at oxygen sites compared with that in Bi and Fe sites. We have also calculated the polarization using the point-charge model and it is found to be around 32% smaller than the actual value. The reduced value of polarization obtained from the point-charge model is related to the covalence effect.

From Table IV it is clear that the polarization values are very much directional dependent (see Table IV). Our calculated value of polarization corresponding to the z direction can be compared with the theoretical values of 84.2 $\mu C/cm^2$ from LSDA,[19] and 98.9 $\mu C/cm^2$ from the LDA+U

method.[29] The large anisotropy in the calculated polarization values indicate that if the samples are aligned along [111], then they will have larger polarization than those aligned along other orientations in the substrate. This could explain why some reports show large value (35.7–158 $\mu C/cm^2$) of polarization in this material and others show very small value (2.2–8.9 $\mu C/cm^2$). We found that the natural value of the polarization is 88.7 $\mu C/cm^2$ along [111] direction, consistent with the recent measurements.[13,16]

IV. SUMMARY

We have reported results from electronic structure calculations for the multiferroic $BiFeO_3$ using generalized gradient corrected accurate density functional calculation. We have found that the *A*-AF-like phase is stable in energy compared to the other magnetic configurations in $BiFeO_3$. This phase sustains ferroelectric rhombohedral distortions with large shifts of Bi atoms, in agreement with the fact that a large portion of the ferroelectric polarization in Bi-based perovskitelike phases is provided by Bi displacements. The stereochemically active lone pair in $BiFeO_3$ causes a symmetry lowering structural distortion which drives the ferroelectric phase transition and, as a secondary effect, allows *A*-AF ordering or the canted spin structure over the *G*-AF ordering. The agreement between the calculated spontaneous polarization (**P**) and recent experimental data demonstrate that the crystal wave functions in the frozen ferroelectric structure convey the essential physics of the spontaneous polarization in real materials. The important observations from our calculations can be summarized as follows.

(1) Unlike earlier calculations, our calculated structural parameters for ferroelectric $BiFeO_3$ are found to be in good agreement with experimental values and especially the experimentally observed rhombohedral angle for this material has been reproduced quantitatively.

(2) Structural stability studies show a pressure induced structural transition from polar $R3c$ structure to the nonpolar orthorhombic *Pnma* structure around 130 kbar. We have also identified two ferroelectric phases such as tetragonal $P4mm$ and monoclinic *Cm* structures at the expanded lattice.

(3) We have observed insulating behavior in both the paraelectric $R\bar{3}c$ phase and the ferroelectric $R3c$ phase without including strong Coulomb correlation effect into the calculations.

(4) Total-energy calculations show large energy difference between different magnetic configurations in $BiFeO_3$ and we found insulating behavior in *A*-AF and *G*-AF configurations and metallic behavior in the nonmagnetic, ferromagnetic and *C*-AF configurations. We believe that GGA itself is sufficient to describe the properties of $BiFeO_3$. However, if correlation effect is significant in this material one could expect that the predicted energetics of different magnetic configurations and electronic behavior will change.

(5) Detailed analysis of the chemical bonding shows that the electrons transfer from both Bi and Fe atoms to the O sites and also finite hybridization interaction takes place between the Bi-O as well as Fe-O. This hybridization interaction plays a dominant role in the large ferroelectric polarization.

(6) The role of Bi lone pair on the chemical bonding and ferroelectric distortion has been analyzed. We found that the lone pair lobe formation is driven primarily by covalency between Bi *s* and O s/p states with the mediation of Bi *p* states rather than the classical picture of hybridization between Bi 6*s* and Bi 6*p* orbitals.

(7) The complete BEC tensor is reported for all the constituents in both the ferroelectric and paraelectric phases using accurate density functional calculations. The calculated BEC at the ferroelectric and the paraelectric phases indicate that the charges are strongly affected by ferroelectric displacement of ions.

(8) Consistent with experimental observation, our calculations shows that the easy axis of polarization is along the [111] direction in $BiFeO_3$. The ferroelectricity in $BiFeO_3$ is originating from the distortion of Bi-O coordination environment as a result of the stereochemical activity of the lone pair on Bi.

(9) Large anisotropy in the polarization of $BiFeO_3$ has been identified and this could explain why there is large scattering in the experimentally reported polarization values in this material.

(10) Our partial polarization analysis demonstrates that the polarization is essentially due to the displacement of Bi relative to the center of the FeO_6 octahedra.

The overall conclusion is that our results are in good agreement with experiment. This demonstrates that accurate density functional calculations can be used to explore not only the structural and magnetic properties but also the ferroelectric properties of magnetoelectric materials.

ACKNOWLEDGMENTS

The authors gratefully acknowledge the Research Council of Norway for financial support under Grant No. 158518/431 (NANOMAT) and for the computer time at the Norwegian supercomputer facilities. P.R. wishes to thank useful communications received from Florent Boucher, Jan Lazewski, Jeffrey Neaton, Karen Johnston, Umesh V. Waghmare, Sergey Prosandeev, Arne Klaveness, and Karel Knizek. The skillful assistance from the staff at Swiss-Norwegian Beam Line, ESRF is gratefully acknowledged.

*Electronic address: ravindran.ponniah@kjemi.uio.no; URL: http://www.folk.uio.no/ravi

[1] M. Fiebig, T. Lottermoser, D. Fröhlich, A. V. Goltsev, and R. V. Pisarev, Nature (London) **419**, 818 (2002).
[2] T. Kimura, S. Kawamoto, I. Yamada, T. Arima, and Y. Takura, Nature (London) **426**, 55 (2003).
[3] *Proceedings of the 5th International Workshop on Magnetoelectric Interaction Phenomena in Crystals*, edited by M. Fiebig, V. Eremenko, and I. E. Chupis (Kluwer, Dordrecht, 2004).
[4] G. A. Smolenskii and I. E. Chupis, Usp. Fiz. Nauk **137**, 415 (1982) [Sov. Phys. Usp. **25**, 475 (1982)].
[5] H. Schmid, Ferroelectrics **62**, 317 (1994).
[6] V. G. Bhide and M. S. Multani, Solid State Commun. **3**, 271 (1965).
[7] J. M. Moreau, C. Michel, R. Gerson, and W. J. James, J. Phys. Chem. Solids **32**, 1315 (1971).
[8] Y. N. Venevtsev and V. V. Gagulin, Inorg. Mater. **31**, 797 (1995).
[9] I. E. Dzyaloshinskii, JETP **32**, 1547 (1957) [Sov. Phys. JETP **5**, 1259 (1957)].
[10] T. Moria, Phys. Rev. **120**, 91 (1960).
[11] I. Sosnowska, T. Peterlin-Neumaier, and E. Steichele, J. Phys. C **15**, 4835 (1982).
[12] Y. F. Popov, A. K. Zvezdin, G. P. Vorob'ev, A. M. Kadomtseva, V. A. Murashev, and D. N. Rakov, Pis'ma Zh. Eksp. Teor. Fiz. **57**, 65 (1993) [JETP Lett. **57**, 69 (1993)].
[13] J. Wang, J. B. Neaton, H. Zheng, V. Nagarajan, S. B. Ogale, B. Liu, D. Viehland, V. Vaithyanathan, D. G. Schlom, U. V. Waghmare, N. A. Spaldin, K. M. Rabe, M. Wutting, and R. Ramesh, Science **299**, 1719 (2003).
[14] J. S. Kim, C. Cheon, Y. N. Choi, and P. W. Jang, J. Appl. Phys. **93**, 9263 (2003).
[15] H. Gu, J. Xue, and J. Wang, Appl. Phys. Lett. **79**, 2061 (2001).
[16] K. Y. Yun, D. Ricinschi, T. Kanashima, M. Noda, and M. Okuyama, Jpn. J. Appl. Phys., Part 2 **43**, L647 (2004).
[17] J. R. Teague, R. Gerson, and W. J. James, Solid State Commun. **8**, 1073 (1970).
[18] J. F. Li, J. Wang, N. Wang, F. Bai, B. Ruette, A. P. Pyatakov, M. Wuttig, R. Ramesh, A. K. Zvezdin, and D. Viehland, Appl. Phys. Lett. **84**, 5261 (2004).
[19] J. B. Neaton, C. Ederer, U. V. Waghmare, N. A. Spaldin, and K. M. Rabe, Phys. Rev. B **71**, 014113 (2005).
[20] C. Ederer and N. A. Spaldin, Phys. Rev. Lett. **95**, 257601 (2005).
[21] C. Michel, J.-M. Moreau, G. D. Achenbach, R. Gerson, and W. J. James, Solid State Commun. **7**, 701 (1969).
[22] F. Kubel and H. Schmid, Acta Crystallogr., Sect. B: Struct. Sci. **46**, 698 (1990).
[23] V. R. Palkar, J. John, and R. Pinto, Appl. Phys. Lett. **80**, 1628 (2002).
[24] Y. P. Wang, L. Zhou, M. F. Zhang, X. Y. Cheng, J.-M. Liu, and Z. G. Liu, Appl. Phys. Lett. **84**, 1731 (2004).
[25] I. Sosnowska, W. Schäfer, W. Kockelmann, K. H. Andersen, and I. O. Troyanchuk, Appl. Phys. A: Mater. Sci. Process. **74**, S1040 (2002).
[26] R. D. King-Smith and D. Vanderbilt, Phys. Rev. B **47**, 1651 (1993); D. Vanderbilt and R. D. King-Smith, *ibid.* **48**, 4442 (1993).
[27] R. Resta, Ferroelectrics **136**, 51 (1992).
[28] S. Baroni, P. Giannozzi, and A. Testa, Phys. Rev. Lett. **58**, 1861 (1987); P. Giannozzi, S. de Gironcoli, P. Pavone, and S. Baroni, Phys. Rev. B **43**, 7231 (1991).
[29] C. Ederer and N. A. Spaldin, Phys. Rev. B **71**, 224103 (2005).
[30] G. Kresse and J. Hafner, Phys. Rev. B **47**, 558 (1993); G. Kresse and J. Furthmuller, Comput. Mater. Sci. **6**, 15 (1996).
[31] P. E. Blöchl, Phys. Rev. B **50**, 17953 (1994).
[32] G. Kresse and D. Joubert, Phys. Rev. B **59**, 1758 (1999).
[33] W. Kohn and L. J. Sham, Phys. Rev. **136**, B864 (1965).
[34] M. C. Payne, M. Teter, D. C. Allen, T. A. Arias, and J. D. Joannopoulos, Rev. Mod. Phys. **64**, 1045 (1992).
[35] P. Pulay, Chem. Phys. Lett. **73**, 393 (1980).
[36] J. P. Perdew, in *Electronic Structure of Solids*, edited by P. Ziesche and H. Eschrig (Akademie Verlag, Berlin, 1991); J. P. Perdew, K. Burke, and Y. Wang, Phys. Rev. B **54**, 16533 (1996); J. P. Perdew, K. Burke, and M. Ernzerhof, Phys. Rev. Lett. **77**, 3865 (1996).
[37] C. Elsässer, M. Fähnle, C. T. Chan, and K. M. Ho, Phys. Rev. B **49**, 13975 (1994).
[38] H. J. Monkhorst and J. D. Pack, Phys. Rev. B **13**, 5188 (1976).
[39] T. Barth, Norsk Geologisk Tidsskrift **8**, 201 (1925).
[40] A. W Hewat, J. Phys. C **6**, 1074 (1973).
[41] G. Thornton, B. C. Tofield, and A. W. Hewat, J. Solid State Chem. **61**, 301 (1986).
[42] G. Maris, Y. Ren, V. Volotchaev, C. Zobel, T. Lorenz, and T. T. M. Palstra, Phys. Rev. B **67**, 224423 (2003).
[43] B. Lampis, P. Sciau, and A. G. Lehmann, J. Phys.: Condens. Matter **11**, 3489 (1999).
[44] P. Bordet, C. Chaillout, M. Marezio, Q. Huang, A. Santoro, S.-W. Cheong, H. Takagi, C. S. Oglesby, and B. Batlogg, J. Solid State Chem. **106**, 253 (1993).
[45] P. Vajeeston, P. Ravindran, A. Kjekshus, and H. Fjellvåg, Phys. Rev. Lett. **89**, 175506 (2002).
[46] P. Vajeeston, P. Ravindran, R. Vidya, A. Kjekshus, and H. Fjellvåg, Appl. Phys. Lett. **82**, 2257 (2003).
[47] S. V. Kiselev, R. P. Ozerov, and G. S. Zhdanov, Dokl. Akad. Nauk SSSR **145**, 1255 (1962) [Sov. Phys. Dokl. **7**, 742 (1963)].
[48] G. P. Vorob'ev, A. K. Zvezdin, A. M. Kadomtseva, Y. F. Popov, V. A. Murashov, and D. N. Rakov, Fiz. Tverd. Tela (S.-Peterburg) **37**, 3262 (1995) [Phys. Solid State **37**, 1793 (1995)].
[49] A. Savin, R. Nesper, S. Wengert, and T. F. Fässler, Angew. Chem., Int. Ed. Engl. **36**, 1808 (1997).
[50] N. N. Krainik, N. P. Khuchua, V. V. Zhdanova, and V. Evseev, J. Phys. C **15**, 4835 (1982).
[51] M. Polomska, W. Kaczmarek, and Z. Pajak, Phys. Status Solidi A **23**, 567 (1974).
[52] R. D. Shannon and C. T. Prewitt, Acta Crystallogr., Sect. B: Struct. Crystallogr. Cryst. Chem. **25**, 925 (1969).
[53] P. Fischer, M. Polomskya, I. Sosnowska, and M. Szymanksi, J. Phys. C **13**, 1931 (1980).
[54] J. D. Bucci, B. K. Robertson, and W. J. James, J. Appl. Crystallogr. **5**, 187 (1972).
[55] Y. E. Roginskaya, Y. Y. Tomashpol'skii, Y. N. Venevtsev, V. M. Petro, and G. S. Zhdanov, JETP Lett. **50**, 69 (1966) [Sov. Phys. JETP **23**, 47 (1966)].
[56] Z. Wu, R. E. Cohen, and D. J. Singh, Phys. Rev. B **70**, 104112 (2004).
[57] Z. Wu and R. E. Cohen, Phys. Rev. Lett. **95**, 037601 (2005).
[58] B. Noheda, J. A. Gonzalo, L. E. Cross, R. Guo, S.-E. Park, D. E. Cox, and G. Shirane, Phys. Rev. B **61**, 8687 (2000).
[59] P. Baettig, C. Ederer, and N. A. Spaldin, Phys. Rev. B **72**, 214105 (2005).
[60] Z. Wu and H. Krakauer, Phys. Rev. B **68**, 014112 (2003).

[61] R. Guo, L. E. Cross, S.-E. Park, B. Noheda, D. E. Cox, and G. Shirane, Phys. Rev. Lett. **84**, 5423 (2000).
[62] J. Iniguez, D. Vanderbilt, and L. Bellaiche, Phys. Rev. B **67**, 224107 (2003).
[63] S. V. Halilov, M. Fomari, and D. J. Singh, Appl. Phys. Lett. **81**, 3443 (2002).
[64] R. E. Cohen and H. Krakauer, Ferroelectrics **136**, 95 (1992); R. E. Cohen, Nature (London) **358**, 136 (1992).
[65] M. Posternak, R. Resta, and A. Baldereschi, Phys. Rev. B **50**, 8911 (1994).
[66] P. Ravindran, P. Vajeeston, R. Vidya, A. Kjekshus, and H. Fjellvåg, Phys. Rev. Lett. **89**, 106403 (2002).
[67] R. E. Cohen and H. Krakauer, Phys. Rev. B **42**, 6416 (1990).
[68] V. V. Nemoshkalenko and A. N. Timoshevskii, Phys. Status Solidi B **127**, 163 (1985); L. T. Hudson, R. L. Kurtz, S. W. Robey, D. Temple, and R. L. Stockbauer, Phys. Rev. B **47**, 1174 (1994).
[69] Ph. Ghosez, X. Gonze, Ph. Lambin, and J. P. Michenaud, Phys. Rev. B **51**, 6765 (1995).
[70] N. A. Hill, J. Phys. Chem. B **104**, 6694 (2000).
[71] M. Atanasov and D. Reinen, J. Phys. Chem. A **105**, 5450 (2001).
[72] O. K. Andersen and O. Jepsen, Phys. Rev. Lett. **53**, 2571 (1984).
[73] R. Dronskowski and P. E. Blochl, J. Phys. Chem. **92**, 5397 (1993).
[74] G. Krier, O. Jepsen, A. Burkhardt, and O. K. Andersen, Tight Binding LMTO-ASA Program Version 4.7, Stuttgart, Germany, 1999.
[75] R. D. King-Smith and D. Vanderbilt, Phys. Rev. B **49**, 5828 (1994).
[76] C. Blaauw and F. van der Woude, J. Phys. C **6**, 1422 (1973).
[77] I. Sosnowska, T. Peterlin-Neumaier, and E. Steichele, J. Phys. C **15**, 4835 (1982).
[78] A. V. Zalesskii, A. A. Frolov, A. K. Zvezdin, A. A. Gippius, E. N. Morozova, D. F. Khozeev, A. S. Bush, and V. S. Pokatilov, J. Exp. Theor. Phys. **95**, 101 (2002).
[79] P. Ravindran, A. Kjekshus, H. Fjellvåg, A. Delin, and O. Eriksson, Phys. Rev. B **65**, 064445 (2002).
[80] S. Nakamura, S. S. Soeya, N. Ikeda, and M. Tanaka, J. Appl. Phys. **74**, 5652 (1993).
[81] B. Silvi and A. Savin, Nature (London) **371**, 683 (1994).
[82] G. W. Watson and S. C. Parker, J. Phys. Chem. B **103**, 1258 (1999); G. W. Watson, S. C. Parker, and G. Kresse, Phys. Rev. B **59**, 8481 (1999).
[83] R. Seshadri, Proc.-Indian Acad. Sci., Chem. Sci. **113**, 487 (2001).
[84] L. E. Orgel, J. Chem. Soc. **1959**, 3815 (1959).
[85] U. V. Waghmare, N. Spaldin, H. C. Kandpal, and R. Seshadri, Phys. Rev. B **67**, 125111 (2003).
[86] B. G. Hyde and S. Andersson, *Inorganic Crystal Structures* (John Wiley, New York, 1989).
[87] J. C. Phillips, Rev. Mod. Phys. **42**, 317 (1970).
[88] J. D. Axe, Phys. Rev. **157**, 429 (1967).
[89] R. Resta, Rev. Mod. Phys. **66**, 899 (1994).
[90] R. Pick, M. H. Cohen, and R. M. Martin, Phys. Rev. B **1**, 910 (1970).
[91] D. Vanderbilt and R. D. King-Smith, Phys. Rev. B **48**, 4442 (1994).
[92] R. Resta, M. Posternak, and A. Baldereschi, Phys. Rev. Lett. **70**, 1010 (1993).
[93] W. Zhong, R. D. King-Smith, and D. Vanderbilt, Phys. Rev. Lett. **72**, 3618 (1994).
[94] M. Lax and E. Burstein, Phys. Rev. **97**, 39 (1955).
[95] M. Born and K. Huang, *Dynamical Theory of Crystal Lattices* (Oxford University Press, Oxford, 1954).
[96] H. Bilz and W. Kress, *Phonon Dispersion Relations in Insulators* (Springer, Berlin, 1979).
[97] J. C. Slater, Phys. Rev. **78**, 748 (1950); J. D. Axe, *ibid.* **157**, 429 (1967).
[98] R. M. Martin, Phys. Rev. B **9**, 1998 (1974).
[99] M. E. Lines and A. M. Glass, *Principle and Applications of Ferroelectrics and Related Materials* (Clarendon, Oxford, 1977).
[100] K. Y. Yun, M. Noda, and M. Okuyama, Appl. Phys. Lett. **83**, 3981 (2003).
[101] R. Seshadri and N. A. Hill, Chem. Mater. **13**, 2892 (2001).
[102] I. Inbar and R. E. Cohen, Ferroelectrics **164**, 45 (1995).